THEORY MANUAL

REDBACK

Rock mEchanics with Dissipative feedBACKs

Thomas Poulet   *Manolis Veveakis*

CSIRO   *UNSW*

Collaborators (in chronological order):
Martin Paesold (UWA)
Mustafa Sari (UNSW)
James Gilgannon (Universität Bern)

November 24, 2017

Contents

1. Introduction

The REDBACK application was developed to model multi-physics *Rock mEchanics with Dissipative feedBACKs* in a tightly coupled manner. It is based on the Multi-physics Object Oriented Simulation Environment MOOSE[1] (Gaston et al., 2009) which proposes a powerful and flexible platform to solve multi-physics problems implicitly and in a tightly coupled manner on unstructured meshes. MOOSE aims at providing a wide range of modules to model various physical phenomena, including rock mechanics, which are as flexible as possible and can be easily coupled together. By comparison, REDBACK is The philosophy behind REDBACK is to focus on a non-dimensional formulation of the problem in order to focus on the physical processes at play

This document is a work-in-progress and does not go into all details. Real applications have recently been published that explain specifically the mechanical model (Poulet et al., 2016 (in press)) and the model including the chemical terms (Poulet and Veveakis, 2016). Any contribution is much welcome, feel free to contact us.

---

[1]http://mooseframework.org

2. Governing equations

2.1. Conventions

In this document we assume that stresses are taken positive in tension and pore pressure is positive ($p_f > 0$). Index notation is used. The indices used are i, j, k, l. All other letters or character-strings appearing as indices belong to the symbol used and are not subject to the index notation rules. REDBACK is using a set of equations that are written for a biphasic material, namely a solid and a fluid phase irrespective of the processes involved, e.g. chemical reactions that produce different kinds of solids and fluids.

2.2. System of equations

The system in its final form is

$$
0 = \partial_j \sigma'_{ij} - \partial_i p_f + b_i, \tag{2.1a}
$$

$$
0 = \partial_t p_f + Pe\, \bar{v}_i^\beta \partial_i p_f - Pe\, \bar{v}_i^\Lambda \partial_i T - \partial_i \left[\frac{1}{Le} \partial_i p_f \right] \tag{2.1b}
$$

$$
- \Lambda_m \partial_t T + \frac{Pe\, \epsilon_V}{\bar{\beta}^*} - \frac{1}{Le_{chem}} \omega_F,
$$

$$
0 = \partial_t T + Pe\, \bar{v}_i^m \partial_i T - \partial_{ii}^2 T - Gr\, \sigma_{ij}^{pl} \dot{\epsilon}_{ij}^{pl} \tag{2.1c}
$$

$$
+ Da_{endo}\, (1-s)(1-\phi) e^{\frac{Ar_F\, \delta T}{1+\delta T}}
$$

$$
- Da_{exo}\, s(1-\phi) \Delta\phi_{chem} e^{\frac{Ar_R\, \delta T}{1+\delta T}}.
$$

All dimensionless groups are defined in Tab. 2.1 and

$$\bar{\beta} = (1 - \phi)\beta_s + \phi\beta_f,$$

$$\bar{\beta}^* = \bar{\beta}\,\sigma_{ref},$$

$$\bar{v}_i^{\beta} = (1 - \phi)\frac{\beta_s}{\bar{\beta}}v_i^s + \phi\frac{\beta_f}{\bar{\beta}}v_i^f,$$

$$\bar{v}_i^{\Lambda} = (1 - \phi)\Lambda_s v_i^s + \phi\Lambda_f v_i^f,$$

$$\bar{v}_i^m = (1 - \phi)\frac{\rho_s}{\bar{\rho}}v_i^s + \phi\frac{\rho_f}{\bar{\rho}}v_i^f,$$

$$\omega_F^* = \frac{\omega_F M_{AB} e^{Ar}}{\rho_{AB} k_F} = (1 - \phi)(1 - s)\exp\left(\frac{Ar_F\,\delta T}{1 + \delta T}\right),$$

$$\dot{\epsilon}_{ij}^{vp} = \dot{\epsilon}_0\,\exp\left(\frac{Ar\,\delta T}{1 + \delta T}\right)\sqrt{\left\langle\frac{q - q_Y}{\sigma_{ref}}\right\rangle^{2m} + \left\langle\frac{p - p_Y}{\sigma_{ref}}\right\rangle^{2m}}\,\frac{\partial f}{\partial\sigma_{ij}}.$$

All symbols are defined in Tab. B.1.

The total porosity ϕ is expressed as the sum of its initial value, ϕ_0, and the newly created interconnected pore volume. For simplicity reasons, all porosity is assumed to be interconnected (or at least up to the point this document was written). Pore volume can be created by mechanical ($\Delta\phi_{mech}$) and chemical ($\Delta\phi_{chem}$) processes such that the total porosity reads

$$\phi = \phi_0 + \Delta\phi_{mech} + \Delta\phi_{chem} = \frac{V_B}{V}, \tag{2.2}$$

where V_B is the volume occupied by fluid B. The evolution of mechanical porosity contains two components, a plastic part $\Delta\phi_{mech}^{vp} = \epsilon_V^{pl}$, with ϵ_V^{pl} the volumetric plastic strain, and an elastic one $\Delta\phi_{mech}^e = (1 - \phi)(\beta_s\Delta p_f - \lambda_s\Delta T)$ where β_s and λ_s are compressibility and thermal expansion coefficients of the solid phase, respectively.

2.3. Rescaling

A particularity of REDBACK is to work with dimensionless parameters, in line with the purpose of studying system stabilities. As such, the variables used in the final system of equation (Eq. 2.1) are all dimensionless and defined as such:

$$p^* = \frac{p_f}{\sigma_{ref}}, \tag{2.3a}$$

$$T^* = \frac{T - T_{ref}}{\delta T_{ref}}, \tag{2.3b}$$

$$x^* = \frac{x}{x_{ref}}, \tag{2.3c}$$

$$t^* = \frac{c_{th}}{x_{ref}^2}t, \tag{2.3d}$$

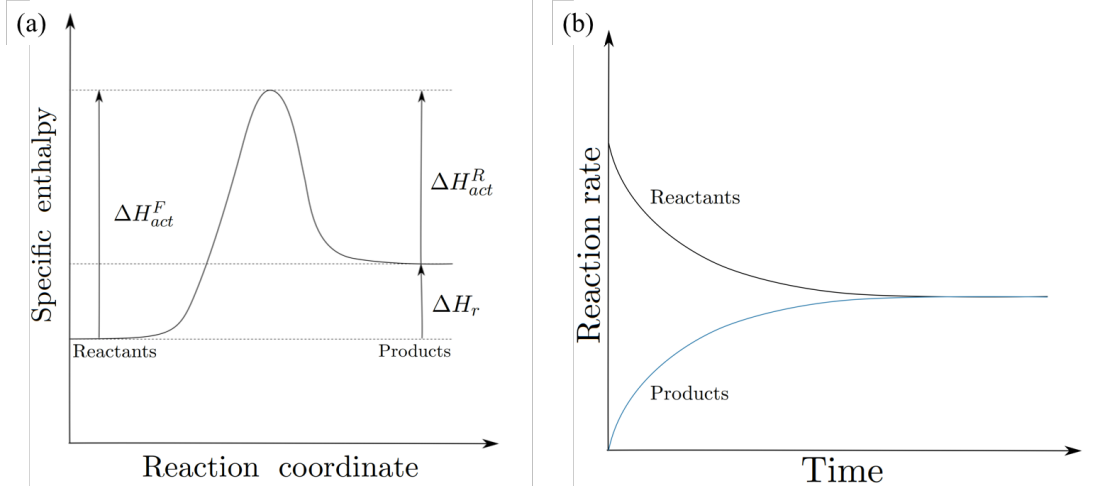$$V^* = \frac{V}{V_{ref}}. \tag{2.3e}$$

Figure 2.1.: (a) Schematic explanation of the activation enthalpies of the forward and reverse reactions, and the enthalpy of the reaction. (b) Evolution of the reaction rates of the reactants (black curve) and the products (blue curve) towards the equilibrium rate.

with $c_{th} = \alpha/(\rho C_p)_m$. The derivations of those dimensionless variables is detailed in Sec. A.

Note that the time can in turn be rescaled a second time for numerical reasons (see Sec. 6.1.1).

2.4. Chemical damage

Thermally activated chemical reactions are allowed to take place and in this work we concentrate on (de-)hydration reactions of the form

$$\zeta_1 AB_s \underset{\omega_R}{\overset{\omega_F}{\rightleftharpoons}} \zeta_2 A_s + \zeta_3 B_f, \tag{2.4}$$

where the subscripts s and f refer to solid and fluid phases and ζ_i ($i = 1, 2, 3$) are stoichiometric coefficients. The reaction equation (2.4) states that the solid A can release/bind the component B into/from the fluid phase which increases/reduces the pore pressure.

The kinetics of the decomposition reaction (2.4) are assumed to follow a standard Arrhenius dependency on temperature (Poulet et al., 2014). As a result, the rates of the forward, ω_F, and reverse reaction, ω_R (let $\zeta_1 = \zeta_2 = \zeta_3 = 1$) can be expressed as (Alevizos et al., 2014)

$$\omega_F = \frac{\rho_{AB}}{M_{AB}}(1 - \phi)(1 - s)k_F e^{-\Delta H_{act}^F/RT}, \tag{2.5a}$$

$$\omega_R = \frac{\rho_A \rho_B}{M_A M_B}(1 - \phi)s\Delta\phi_{chem}k_R e^{-\Delta H_{act}^R/RT}, \tag{2.5b}$$

where ρ_i and M_i $(i = A, B, AB)$ are the densities and molar masses of the respective constituent, k_F, k_R, $\Delta H_{act}^F, \Delta H_{act}^R$ are the pre-exponential factors and activation enthalpies of the forward and reverse reaction, ϕ is porosity and $\Delta\phi_{chem}$ denotes change in porosity due to chemical processes. We define the solid ratio

$$s = \frac{V_A}{V_s} = \frac{V_A}{(1-\phi)V}, \tag{2.6}$$

where V is a representative volume, V_A and V_s is the volume of solid phase A and all solid within V, respectively. The solid ratio is a measure of the extend of reaction (2.4). Subsequently, the total reaction rate is

$$\omega = \left[(1-s) - s\Delta\phi_{chem} \frac{\rho_A \rho_B}{\rho_{AB}^2} \frac{M_{AB}^2}{M_A M_B} K_c^{-1} e^{\Delta H_r/RT} \right] (1-\phi) \frac{\rho_{AB}}{M_{AB}} k_F e^{-\Delta H_{act}^F/RT} \tag{2.7}$$

where $K_c = k_F/k_R$ and $\Delta H_r = \Delta H_{act}^R - \Delta H_{act}^F$. The expressions for the dependency of the porosity ϕ and solid ratio s on the reaction kinetics are described in detail in Alevizos et al. (2014) and briefly summarized here.

We assume the following relations for the partial molar reaction rates of the species involved

$$\omega_{AB} = -\left[\frac{\rho_{AB}}{M_{AB}}(1-\phi)(1-s) \right]^{\zeta_1} k_F \exp(-\Delta H_{act}^F/RT), \tag{2.8a}$$

$$\omega_A = \left[\frac{\rho_A}{M_A}(1-\phi)s \right]^{\zeta_2} k_A \exp(-\Delta H_{act}^R/RT), \tag{2.8b}$$

$$\omega_B = \left[\Delta\phi_{chem} \frac{\rho_B}{M_B} \right]^{\zeta_3} k_B \exp(-\Delta H_{act}^R/RT), \tag{2.8c}$$

and those rates are linked by the stoichiometry of the considered reaction (2.4) as

$$-\frac{\omega_{AB}}{\zeta_1} = \frac{\omega_A}{\zeta_2} = \frac{\omega_B}{\zeta_3}. \tag{2.9}$$

From Eqs. (2.8-2.9) and for $\zeta_1 = \zeta_2 = \zeta_3 = 1$ we derive the poro-chemical model

$$\Delta\phi_{chem} = A_\phi \frac{1-\phi_0}{1 + \frac{\rho_B}{\rho_A}\frac{M_A}{M_B}\frac{1}{s}}, \tag{2.10a}$$

$$s = \frac{\omega_{rel}}{1 + \omega_{rel}}, \tag{2.10b}$$

$$\omega_{rel} = \frac{\rho_{AB}}{\rho_A}\frac{M_A}{M_{AB}} K_c \exp\left(\frac{\Delta H_r}{RT} \right), \tag{2.10c}$$

where A_ϕ is a coefficient that determines the amount of the interconnected pore-volume (porosity) created due to the reaction. We assume that all the fluid generated contributes to the interconnected pore volume, and thus set $A_\phi = 1$.

Table 2.1.: Dimensionless parameters used in REDBACK. The coefficient δ is defined such that $T^\star = (T - T_{ref})/(\delta T_{ref})$

Group	Name	Definition	Interpretation
Gr	Gruntfest number	$\frac{\chi \sigma_{ref} \dot{\epsilon}_{ref} x_{ref}^2}{\alpha \delta T_{ref}}$	ratio of mechanical rate converted into heat over rate of diffusive processes
Da_{endo}	Endothermic Damköhler number	$\frac{A_{endo} h_{endo} \rho_{AB} x_{ref}^2}{\alpha \delta T_{ref}}$	ratio of endothermic reaction rate over rate of diffusive processes
Da_{exo}	Exothermic Damköhler number	$\frac{A_{exo} h_{exo} \rho_{AB} x_{ref}^2}{\alpha \delta T_{ref}}$	ratio of exothermic reaction rate over rate of diffusive processes
Ar	Arrhenius number	$\Delta H_{mech}/(RT_{ref})$	Ratio of activation enthalpy over thermal energy
Ar_F	Forward Arrhenius number	$\Delta H_{act}^F/(RT_{ref})$	Ratio of activation enthalpy of forward reaction over thermal energy
Ar_R	Reverse Arrhenius number	$\Delta H_{act}^R/(RT_{ref})$	Ratio of activation enthalpy of reverse activation energy over thermal energy
Le	Lewis number	$c_{th}/c_{hy} = \frac{\mu_f \, c_{th} \, \beta_m^*}{\kappa \, \sigma_{ref}}$	Ratio of thermal over mass diffusivities
Le_{chem}	Chemical Lewis number	$\frac{c_{th} \sigma_{ref} \beta_m}{x_{ref}^2 A_{endo}} \frac{\rho_B}{\rho_{AB}} \frac{M_{AB}}{M_B} \left(\frac{\rho_B}{\rho_f} - \frac{\rho_B}{\rho_s} \right) e^{-Ar_F}$	Ratio of thermal over chemical diffusivity of forward reaction
$\bar{\Lambda}_a$	Thermal pressurisation coefficient of a	$\frac{\lambda_a}{\beta_m} \frac{\delta \, T_{ref}}{\sigma_{ref}}$	Normalised thermal pressurisation coefficient, with λ_a the thermal expansion of a and β_m the mixture's compressibility
Pe	Péclet number	$x_{ref} V_{ref}/c_{th}$	Ratio of temperature advection rate over diffusion rate

3. Flow Laws

The coupling of boundary condtions (p,T) and different physical processes (dissolution-precipitation, dislocation & diffusion creep) affects materials in different ways. Experimentalists have constrained relationships for single behaviours by generating, process appropriate, flow laws to describe the realtionships between physical quantities like stress, strain and temperature. In natural samples it is common for many mechanisms to act congruently and as such a single flow law may be inappropriate to describe the physics at play. We have utilised a UserObjectBase Class to implement Flow Laws. This architecture allows for the creation of composite Flow Laws that capture multipule processes at work.

The UserObjectBase is called RedbackFlowLawBase and is characterised as always have an exponential Arrhenius term $\left(\frac{-Q}{RT}\right)$.

It is then possible to create flow laws from this BaseClass that are unique to the physical process that will be active in the model being generated.

When multipule processes are acitve, composite flow laws can be generated. This does require the single process flow laws to be gerenated as a child of the RedbackFlowLawBase first. If the processes are not dependant on each other the they should be solved in seires. For example, dislocation creep and diffusion creep:

$$\dot{\varepsilon}_{tot} = \dot{\varepsilon}_{dis} + \dot{\varepsilon}_{dif}$$

If the processes are dependant they should be solved in parallel. For example, the process of grain boundary sliding is dependant on the process of diffusion creep:

$$\frac{1}{\dot{\varepsilon}_{tot}} = \frac{1}{\dot{\varepsilon}_{dif}} + \frac{1}{\dot{\varepsilon}_{gbs}}$$

These composite flow laws can be combined even further. For example, we know that dislocation creep acts independantly of diffusion creep but diffusion creep may have several active processes dependant on it. Therefore we can say:

$$\dot{\varepsilon}_{tot} = \dot{\varepsilon}_{dis} + \left(\frac{1}{\frac{1}{\dot{\varepsilon}_{dif}} + \frac{1}{\dot{\varepsilon}_{gbs}}}\right)$$

3.1. Normalisation

In an effort to reduce the differences in the orders of magnitudes between units for calculations, the flow laws are made dimentionless by a series of normalising operations.

The reference units used are:

- $\sigma_{ref} = 1e^6$ # reference stress (Pa)

- $d_{ref} = 1e^{-6}$ # reference grain size (m)

- $T_{ref} = 800$ # reference temperature $(°C)$

- $x_{ref} = 1e^{-2}$ # reference size, usually model size (m)

- $c_{th} = 800$ # thermal diffusivity (m^2/s)

- $t_{ref} = x^2_{ref}/c_{th}$ # reference time (s)

1) Dislocation creep of form:

$$\dot{\varepsilon}_{dis} = A_{dis}\sigma_d^n exp^{\left(\frac{-Q_{dis}}{RT}\right)}$$

(3.1)

Note;

A_{dis} units are $\text{MPa}^{-n}\text{s}^{-1}$

Normalisation operations:
$Ar_{dis} = \left(\frac{Q_{dis} \cdot 1e^3}{RT_{ref}}\right)$

$A^*_{dis} = A_{dis}\left(\sigma_{ref} \cdot 1e^{-6}\right)^n t_{ref}exp^{-Ar_{dis}}$

$T^* = \left(\frac{T-T_{ref}}{\delta T_{ref}}\right)$

$\sigma^* = \left(\frac{\sigma_d \cdot 1e^6}{\sigma_{ref}}\right)$

Normalised flow law:

$$\dot{\varepsilon}^*_{dis} = A^*_{dis}\sigma^{*n}exp^{\left(\frac{Ar_{dis}\delta T^*}{(1+\delta)T^*}\right)} \tag{3.2}$$

2) Dislocation creep of form:

$$\dot{\varepsilon}_p = A_p\sigma_d^2 exp^{\left(\frac{\sigma_d}{\sigma_p}\right)}exp^{\left(\frac{-Q_p}{RT}\right)} \tag{3.3}$$

Where;

$$\sigma_p = \left(\Sigma_{p,0} + Kd^{-0.5}\right)\left(T_m - T\right)$$

Note that;

A_p units are $MPa^{-2}s^{-1}$

$\Sigma_{p,0}$ & K units are $MPa\ kK^{-1}$ & $MPa\ kK^{-1}\mu m^{0.5}$

T_m & T are in Kelvin for this flow law

Normalisation operations:
$$Ar_p = \left(\frac{Q_p \cdot 1e^3}{RT_{ref}}\right)$$

$$A^*_p = A_p\left(\sigma_{ref} \cdot 1e^{-6}\right)^2 t_{ref}exp^{-Ar_p}$$

$$T^* = \left(\frac{T - T_{ref}}{\delta T_{ref}}\right)$$

$$\sigma^* = \left(\frac{\sigma_d \cdot 1e^6}{\sigma_{ref}}\right)$$

$$\sigma^*_p = \left(\frac{\sigma_p \cdot 1e^3}{\sigma_{ref}}\right)$$

Normalised flow law:

$$\dot{\varepsilon}^*_p = A^*_p\sigma^{*2}exp^{\left(\frac{\sigma^*}{\sigma^*_p}\right)}exp^{\left(\frac{Ar_p\delta T^*}{(1+\delta)T^*}\right)} \tag{3.4}$$

4. Grain-size sensitivity

4.1. Theory

What follows is a work flow of relevant from the 22/08/16 (James Gilgannon)

At depths in the crust great enough to yeild pressure insensitve material responses, the rheological behaviour of a rock can be considerd to be governed by the average grain-size of the sample (insert ref). In Nature this is manifest by the development of a ductile fault rock series known as a mylonite series. During deformation strain is localised into the zones of finer grain-sizes (acheived due to the deformational condtions). Therefore any modelling approach interested in investigsting strain softening behaviour in rocks requires an robust inegration of a deformationally induced grain-size evoltuion. For this purpose we have chosen to implement the Paleowattmeter of (Austin and Evans, 2007) which describes the evoltuion of grain-size as a function of the deformation condtions.

Austin and Evans (2007) propose that druing deformation the average grain-size of a sample ($\bar{d}$) evolves to a steady state grain-size (d_{ss}) faster than any stress preturbations. With respect to the grain-size evolution, they suggest that a steady state grain-size is acheived when the sum of the rates of growth and redcution are balanced, i.e. equal 0:

$$\dot{d}_{tot} = \dot{d}_{red} + \dot{d}_{growth} \tag{4.1}$$

Where $\dot{d}_{red}$ and $\dot{d}_{growth}$ are:

$$\dot{d}_{red} = \frac{\beta \lambda \sigma_d \dot{\varepsilon} d^2}{c\gamma} \tag{4.2}$$

$$\dot{d}_{growth} = K_g exp^{\left(\frac{-Q_g}{RT}\right)} p^{-1} d^{1-p} \tag{4.3}$$

Therefore;

$$\dot{d}_{tot} = \left(\frac{\beta \lambda \sigma_d \dot{\varepsilon} d^2}{c\gamma}\right) + \left(K_g exp^{\left(\frac{-Q_g}{RT}\right)} p^{-1} d^{1-p}\right) \tag{4.4}$$

Table 4.1.: List of parameters used in grain-size evolution loop. User defined values relate to CALCITE.

Symbol	Name & Description	Definition	Assumptions
X_{dif}	Diffusion subscript		
X_{dis}	Dislocation subscript		
$\dot{d}_{tot}$	The summation of competing rates of changes in grain-size	$\dot{d}_{tot} = \dot{d}_{red} + \dot{d}_{growth}$	When $\dot{d}_{tot} = 0$, then stable grain-size is achieved
$\dot{d}_{red}$	The rate of grain-size reduction	$\frac{\beta\lambda\sigma_d\dot{\varepsilon}d^2}{c\gamma}$	
β	The portion of power dissipated by dislocation creep	$\frac{\dot{W}_{dis}}{\dot{W}_{tot}} = \frac{\sigma\dot{\varepsilon}_{dis}}{\sigma\dot{\varepsilon}_{dis}+\sigma\dot{\varepsilon}_{dif}}$	The stress used is the differential stress!
λ	Constant for energy produced by defect production that is stored in the microstructure	$\lambda = \lambda_{dis} = 0.1; where, \lambda_{dif} = 0$	The value of the constant is derived from experimental work that showed 90% of mechanical work is converted into heat (Austin and Evans, 2009)
σ_d	Differential stress	$\sigma_1 - \sigma_3$	
$\dot{\varepsilon}$	Strain rate	$\frac{d\varepsilon}{dt}$	
d	Grain-size at the increment of calculation		Initial grain-size must be determined by the user
c	Geometric constant	π	Grains are assumed to be spherical (Austin and Evans, 2009)
γ	Constant for grain-boundary energy	$\gamma = 1Jm^{-2}$	Value for γ taken from Covey-Crump (1997)
$\dot{d}_{growth}$	The rate of grain-size growth	$K_g exp^{\left(\frac{-Q_g}{RT}\right)}p^{-1}d^{1-p}$	
K_g	Grain growth pre-exponent	$K_g = 2.5x10^9\mu m^p s^{-1}$ (Covey-Crump, 1997)	
Q_g		$Q_g = 175kJmol^{-1}$ (Covey-Crump, 1997)	
R	Gas constant	$R = 8.314JK^{-1}mol^{-1}$	
p	Grain growth exponent	$p = 3$ (From Covey-Crump (1997) chosen by Herwegh et al. (2014))	
d_{ss}	Steady state grain size	$d_{ss} = \kappa\sigma_d^{-m'}exp^{-\left(\frac{Q'}{RT}\right)}$	
κ		$\left[\frac{c\gamma K_g}{\lambda p K_{dis}}\right]^{\frac{1}{p+1}}$	K_{dis} is the dislocation creep flow law's pre-exponent
m'		$\left[\frac{n+1}{p+1}\right]$	
Q'		$\frac{Q_g-Q_{dis}}{p+1}$	Q_{dis} is the dislocation flow law's activation energy

If ,

$$\dot{d}_{tot} = 0 = \left(\frac{-\beta \lambda \sigma_d \dot{\varepsilon} d^2}{c\gamma} \right) + \left(K_g exp^{\left(\frac{-Q_g}{RT} \right)} p^{-1} d^{1-p} \right) \tag{4.5}$$

and the rock deforms by powerlaw creep then,

$$\dot{\varepsilon}_{dis} = K_{dis} \sigma_d^n exp^{\left(\frac{-Q_{dis}}{RT} \right)} \tag{4.6}$$

Austin and Evans (2007) propose that steady state grain-size can be expressed by:

$$d_{ss} = \kappa \sigma_d^{m'} exp^{\left(\frac{-Q_I}{RT} \right)} \tag{4.7}$$

Please refer to Table 4.1 for detailed explaination of the paramters of Eq. 4.4 & 4.7.

Note: In Austin and Evans (2007) Eq.10 contians error in κ formulation, ε_0 is actually K_{dis}. See Herwegh et al. (2014) Eq.16 for the correct formulation of κ. This document contains the correct term definitions.

4.2. Grain-size evolution loop

The loop below (Fig. 4.1) implements the theory from section 4.1. At each timestep the grain-size is compared to the predicted steady state grain-size expected for the modelled deformation conditions. This loop is repeated at each timestep until the observed grain-size is equal to the expected grain-size for steady state. See Table 4.1 for the defintions of terms used in loop.

The loop is implemented with an AuxKernel (RedbackGrainSizeAux) that updates an AuxVariable ("grain size"). The input file requires the user to asign a few things:

1. a UserObjectFlowLaw. This is composite flow law, it must contain at least one dislocation and one diffusion flow laws with in it. With in each flow law the user will provide the relevant normalised parameters.

2. a UserObjectDislocationFlowLaw must also be provided. This is required for the calculation of $\dot{\varepsilon}_{dis}$ (THIS FLOW LAW WILL BE ASKED FOR AGAIN IN THE

MATERIAL). The user will provide the relevant normalised parameters for the flow law.

> Note: The code should be reviewed to removed the need for the UserObject-DislocationFlowLaw to be entered twice.

3. a grain size AuxVariable. The inital condtions for the AuxVariable will be set in the InitialCondition

4. a Variable for temperature, "temp".

> Note: Temperature in loop has dimentions but the code uses a dimensionless normalisation. TO DO! CODE LOOP TO NORMALISE TEMPERATURE. 4.3e7*math.pow(1e6,1.1)*1e-2*math.pow(1e-6, -3.3)*math.exp(-2e5/(8.3*300))

4.2.1. Further work on grain-size evolution

A couple of weakness exsit in the current implementation of a grain-size evoultion law. Below is bullet points on areas to imporve:

1. The current model intputs a $\bar{d}$ & a variance (2σ) for each finite element. This is based on a gaussian log normal distubtion. However this fails to address a realsitic bias to small grain-sizes. Hence underestimating the contrubtion of diffusion creep.

> Is $\bar{d}$ actually the mean? Is it infact the mode? How do we better account for the real grain-size distrubtions observed in nature?

2. The stored enegry in the microstructure (λ) is currently pre-defined. This pre-scribed constant is infered from experimental observations of 90% heat dissipa-tion. Is this correct to prescribe a λ value? It seems more appropriate to include a dissipation term that incorperates the active micro-mechanisms. Huang et al. (2009) attempt to resolve a grain's dissipated energy into microstructrally appro-priate terms (see their Eq.1). Integrating this approach may be more robust (with a mind to expand the W_{AN} to include the current Dynamic Recovery & Dynamic Recrystallisation along side a Plastic Cavitation term).

3. Both point 1 & 2 address issues with modelling at a continumm scale. With respect to understanding emergent two phase rheologies (sheet silicate rich rocks) and ultimately the development of IWL (Handy, 1994) the problem probaly requires a grainscale evaluation of a evolution law that can be homogenised and upscaled.

Figure 4.1.: Grain-size evolution loop
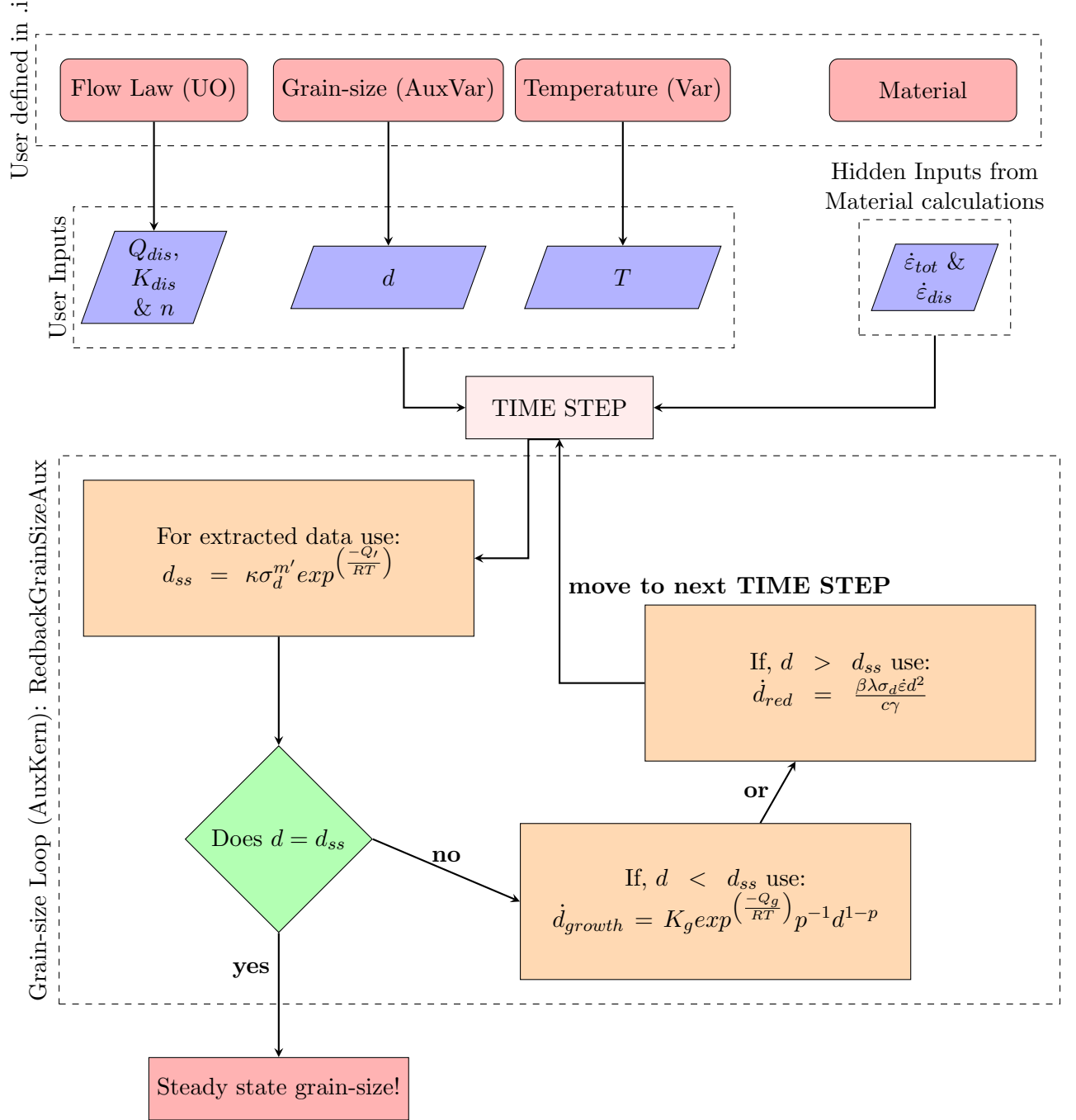
5. Evolution of a second phase

Read MOOSE for phase feild modelling

6. Code architecture

6.1. Kernels

Here is the list of all kernels implemented in REDBACK to solve the system of Eq. 2.1:

$$0 = \overbrace{\partial_j \sigma'_{ij} - \partial_i p_f + b_i}^{\text{RedbackStressDivergenceTensor}},$$

$$0 = \overbrace{\partial_t p_f}^{\text{TimeDerivative}} + \overbrace{Pe\, v_i^p \partial_i p_f - Pe\, v_i^T \partial_i T}^{\text{RedbackMassConvection}} - \overbrace{\partial_i \left[\frac{1}{Le} \partial_i p_f \right]}^{\text{RedbackMassDiffusion}}$$

$$- \underbrace{\Lambda \partial_t T}_{\text{RedbackThermalPressurization}} + \underbrace{\frac{Pe\, \dot{\epsilon}_V}{\bar{\beta}\, \sigma_{ref}}}_{\text{RedbackPoromechanics}} - \underbrace{\frac{1}{Le_{chem}} \omega_F}_{\text{RedbackChemPressure}},$$

$$0 = \underbrace{\partial_t T}_{\text{TimeDerivative}} + \underbrace{Pe\, \bar{v}_i \partial_i T}_{\text{RedbackThermalConvection}} - \underbrace{\partial_{ii}^2 T}_{\text{RedbackThermalDiffusion}} - \underbrace{Gr\, \sigma_{ij}^{pl} \dot{\epsilon}_{ij}^{pl}}_{\text{RedbackMechDissip}} + \underbrace{Da_{endo}\, \omega_F}_{\text{RedbackChemEndo}} - \underbrace{Da_{exo}\, \omega_R}_{\text{RedbackChemExo}}.$$

Note that this expression of the system of equation does not include the time rescaling factor (see following Sec. 6.1.1), which explains the presence of a RedbackThermalDiffusion kernel instead of using the default Diffusion kernel from MOOSE.

6.1.1. Time rescaling

The time used in REDBACK is dimensionless and defined in Eq. 2.3. For numerical reasons however, it can sometimes be useful to rescale time again by introducing t' such that

$$t^* = t' \times \text{time\_factor}. \tag{6.1}$$

Using the newly defined time t' is equivalent to multiplying all the kernels, other than the time derivatives, of Eq. 2.1b and Eq. 2.1c by *time_factor*. This functionality is required

for cases when the initial residual computation is too low and prevents MOOSE from converging to an accurate solution. It is convenient in those cases (e.g. for convection simulations) to use a large factor *time_factor* to increase the initial value of the residual and therefore allow MOOSE to improve that residual down to a low value which will ensure enough numerical precision.

The *time_factor* is defined for each kernel concerned but should only be input as a global variable in your input file.

```
[GlobalParams]
  time_factor = 1.e-3
[]
```

Note that the real time t is then related to the time t' used in the REDBACK simulations by

$$t = \text{time\_factor} \times \frac{x_{ref}^2}{c_{th}} t' \tag{6.2}$$

6.2. Porosity

Porosity plays a particular role as its evolution depends on the mechanical, thermal, and hydraulic process models. As such, the total porosity evolution can not be handled within a material class unfortunately since it has components updated in more than one material. With the RedbackMechMaterial class already derived from the RedbackMaterial class, we can not create a dependency the other way around as it would create a circular dependency problem. There are at least two ways of working around that problem:

1. Porosity can be treated as an extra variable to solve for.

2. Porosity can be treated as an AuxKernel, which allows us to update it with various components calculated in separate material, and yet have all materials use the total porosity (updated with delay obviously).

In the first case the porosity evolution (and dependency on all process models) will be solved rigorously, but this will come at a greater computational cost. This is probably the neatest solution to handle the most generic case when porosity might be strongly dependent on all process models, but this is not the principal scenario we are aiming with the current development of Redback. We are indeed focusing on the case described in Sec. 2, where the porosity is much more strongly dependent on chemistry (which produces fluid and can therefore raise ϕ to 1) than it is on temperature and pore pressure (inducing minor variations of ϕ). As a result, we decided to implement the second option and handle the total porosity as an AuxVariable updated by an AuxKernel. This option provides more flexibility to compute the total porosity more or less accurately by updating the AuxKernel more or less frequently. At the moment we're treating the porosity in an explicit manner and only update it at the end of each step. This is equivalent to say that we neglect the mechanical update of the porosity during a single

step and only consider its chemical variation (since it is the main evolution for the cases we consider).

7. Tests

REDBACK is tested through a series of tests based on various benchmarks for all physical processes involved: thermal (**T**), hydraulic (**H**), mechanical (**M**), and chemical (**C**). All tests are found in the `redback/tests` directory

7.1. Benchmark 1 - T

This benchmark (`redback/tests/benchmark_1_T`) looks at the temperature equation

$$\frac{\partial T}{\partial t} = \frac{\partial^2 T}{\partial x^2} + Gr.e^{\frac{Ar.\delta.T}{1+\delta.T}}. \tag{7.1}$$

The steady state solution is a generalisation of the classical Bratu problem (Bratu, 1914) and is controlled by the Gruntfest number Gr. Using a bifurcation method (Succombe, 2015) we can find the critical value of the Gruntfest number as shown on Fig. 7.1

This problem is then solved using MOOSE on a generated 1D mesh from -1 to 1 for different values of Gr and the initial solution of the temperature T_0 in the center:

- $Gr = 0.095$ and $T_0 = 0$. In this case, the system should converge increasingly to a centre temperature $T_a \approx 0.109$. This case is treated with the input file `bench1_a.i`

- $Gr = 0.095$ and $T_0 = 0.15$. In this case, the system should converge decreasingly to the same centre temperature $T_b = T_a \approx 0.109$. This case is treated with the input file `bench1_b.i`

- $Gr = 0.095$ and $T_0 = 0.25$. In this case, the system should converge increasingly to a large temperature $T_c > 1000$. This case is treated with the input file `bench1_c.i`

- $Gr = 0.1$ and $T_0 = 0$. In this case, the system should converge increasingly to an even larger temperature $T_d > T_c > 1000$. This case is treated with the input file `bench1_d.i`

The numerical results match the theory with the time evolutions shown on Fig. 7.2.

7.2. Benchmark 6 - TM
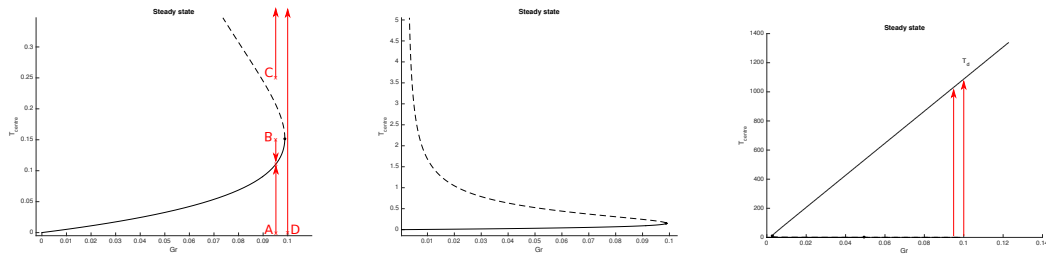
Those benchmarks look at thermal-mechanical simulations.

Figure 7.1.: "S-curve" of the steady state analysis for `benchmark_1_T` with a) zoom on low values of temperatures, showing the four starting conditions and their expected time evolution, b) zoomed out view of the unsteady branch of the "S-curve" in dashed line, and c) even more zoomed out view for larger values of temperatures, showing the higher steady branch where benchmarks C and D converge.
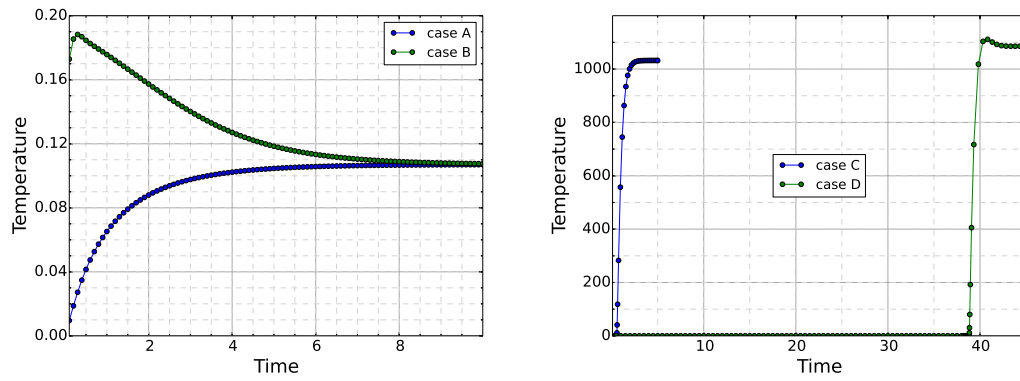

Figure 7.2.: Time evolution of the numerical results for the four benchmarks: a) cases A and B converge to the lower stable branch (see Fig. 7.1), while b) cases C and D converge to the upper stable branch.
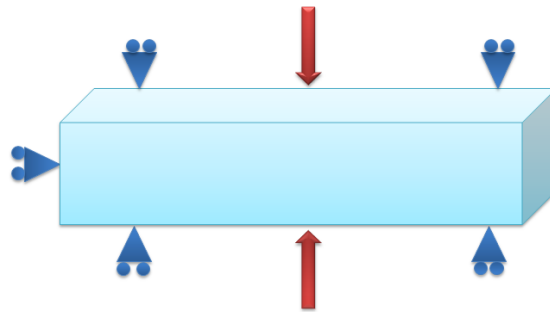

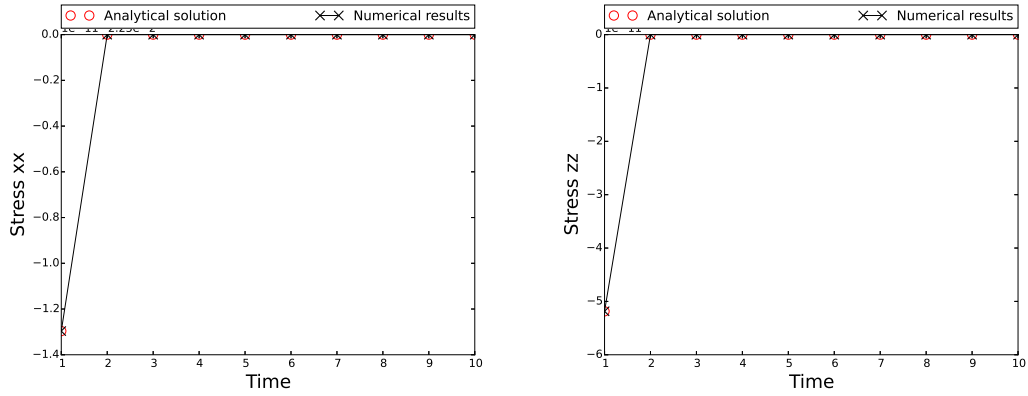Figure 7.3.: This is a caption confining from its sides and the bottom

Figure 7.4.: the effect of thermal stress

7.2.1. Problem Description

by heating of an elastic rod from the back and the front ,this the rod confined in all sides except the top As shown in fig 7.5

.

7.2.2. Analytical solution

The stress in x-axis will be similar to the stress in y-axis whereas the stress in z-axis will be zero since its not confined. because the temperature is increased the rod will expand in z-axis(strain in zz) and that strain calculated by this equation:

$$\varepsilon_{zz} = \frac{\alpha}{2}\Delta T \tag{7.2}$$

we divided α by 2 because in this problem we have two dimension (area thermal expansion coefficient) for more information visit this website om that strain we can caculate the stress in x-axis which is as shown in the equation bellow:

$$\sigma_{xx} = \frac{3}{2}\frac{E}{(1-2\nu)}\frac{\alpha}{2}\Delta T \tag{7.3}$$

Let's explain this step in details...
$\frac{3}{2}$ is the geometric factor

7.2.3. Numerical solution

This problem is then solved using moose on a generated 3D mesh and a comparison of the numerical results against the analytical solution are shown in the figure bellow.

7.3. Benchmark 7 - HM

Those benchmarks look at hydro-mechanical simulations.

Figure 7.5.: Model setup for benchmark 7.3.1 showing applied boundary conditions, with all faces but the top constrained in normal displacement, and an applied downwards velocity on the top face.

7.3.1. Elastic

This benchmark (`redback/tests/benchmark_7_ HM`) looks at Undrained odometer test (in finite strain) to compare with MOOSEporomechanics test (Infinitesimal strain).

7.3.1.1. Problem Description

A cubic single-element fully-saturated sample has roller BCs applied to its sides and bottom. All the sample's boundaries are impermeable. A constant downwards (normal) velocity,v_z, is applied to its top, and the rise in porepressure and effective stress is observed. (Here z denotes the direction normal to the top face.) There is no fluid flow in the single element. Under these conditions, and denoting the height (z length) of the sample by L. As shown in fig 7.5

7.3.1.2. Analytical Solution

To calculate the change in the pore pressure we used this equation

$$P_{\text{f}} = -\frac{TimeFactor}{(1 - \phi)} \left(v_z t/L\right) \tag{7.4}$$

and for the time factor just read 6.1.1 for more details Lets explain this in details:

- To calculate the mass balance to mixture(solid and liquid)we add Eq: A.5 and Eq: A.8 together so we end up with equation (2.1 b)and we solve for isothermal and no convection and no chemical affection and that's lead to the equation bellow:

- $\partial_t p_f = -\frac{Pe\,\dot{\epsilon}_V}{\bar{\beta}\,\sigma_{ref}}$ and from Tab. 2.1 for dimensionless the equation become

  $\partial_t p_f = -\frac{Pe\,\dot{\epsilon}_V}{\beta_s(1-\phi)}$

Also we used the finite strain theory (Coussy, 2004, p.6-7) to calculate the strain in x,y directions,)whereas Moose Poromechanics use infinitesimal transformation theory.

$$\sigma_{xx}^{\text{eff}} = (K - \tfrac{2}{3}G) \left[(v_z t/L) + \left(\frac{1}{2}\,(v_z t/L)^2\right)\right] \ . \tag{7.5}$$

$$\sigma_{zz}^{\text{eff}} = (K + \tfrac{4}{3}G) \left[(v_z t/L) + \left(\frac{1}{2}\,(v_z t/L)^2\right)\right] \ . \tag{7.6}$$
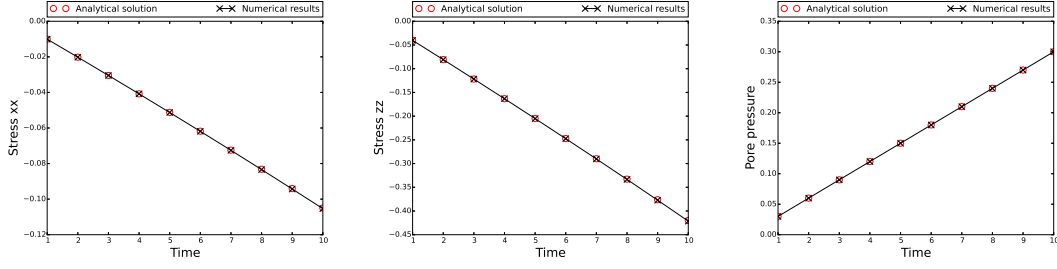
Figure 7.6.: Comparison of analytical vs numerical results for benchmark 7.3.1

7.3.1.3. Numerical Solution

This problem is then solved using moose on a generated 3D mesh for the values bellow:

- Young's modulus $(E) = 3.6$

- Poisson's ratio $(\nu) = 0.2$

- $\Phi = 0.1$

- $L = 1$

- Biot Coefficient $(\alpha) = 0.3$

- Péclet number $(Pe) = 1$

- solid compressibility $(\beta_s) = 3.7037$

- top velocity $(V_z) = 0.01$

In moose poromechanics they used Bulk modulus(K) and shear modulus(G) where:

$$E = \frac{9KG}{3K + G} \tag{7.7}$$

$$\nu = \frac{3K - 2G}{2(3K + G)} \tag{7.8}$$

A comparison of the numerical results against the analytical solution are shown in fig 7.6

7.3.2. Elastic No Porosity

The porosity is kept constant so it is same as the above problem(Elastic)but with changing in the properties :
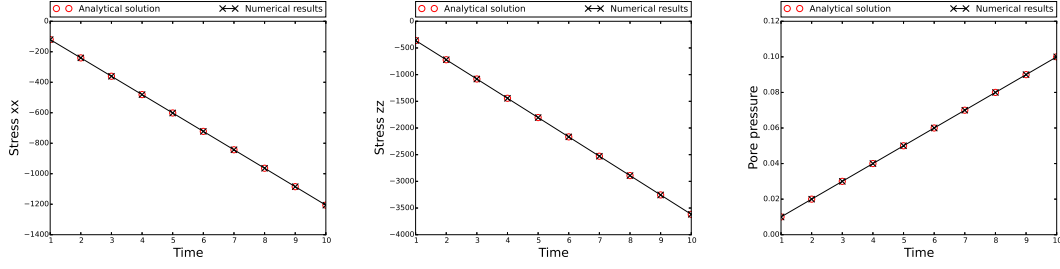
- $E = 3.6$

- $\nu = 0.2$

26

Figure 7.7.: Comparison of analytical vs numerical results for benchmark 7.3.2

- $\Phi = 0.1$

- $L = 1$

- $\alpha = 0.3$

- $Pe = 0.0000009$

- $\beta_s = 0.000001$

- $V_z = 0.01$

A comparison of the numerical results against the analytical solution are shown in Fig. 7.7.

7.3.3. Elastic Porosity

In this problem the porosity evolves according to Eq. A.7 and that equation may be solved in closed form to calculate the small changes in porosity

$$\phi = \phi_o + (1 - \phi)\left[\phi_0 + \beta_s(p - p_o) - \epsilon_v\right] \ . \tag{7.9}$$

Let's explain this step in details...

- by ignoring the convection from Eq. A.7 we end up with

$$(1 - \phi)\frac{\partial \rho_s}{\partial t} - \rho_s \frac{\partial \phi}{\partial t} + \rho_s \frac{\partial((1 - \phi)V_k^{(1)})}{\partial x_k} = 0 \tag{7.10}$$

  by simplifying the above equation we end up with

-
$$(1 - \phi)\frac{\partial \rho_s}{\partial t} + \rho_s \frac{\partial(1 - \phi)}{\partial t} + \rho_s(1 - \phi)\frac{\partial V_k^{(1)}}{\partial x_k} + \rho_s V_k^{(1)}\frac{\partial(1 - \phi)}{\partial x_k} = 0 \tag{7.11}$$

  The last term the equation above is zero since we assume that we have one cell and the porosity is constant with space. so we will end up with

27

-
$$(1 - \phi)\frac{\partial \rho_s}{\partial t} + \rho_s \frac{\partial (1 - \phi)}{\partial t} + \rho_s (1 - \phi)\frac{\partial V_k^{(1)}}{\partial x_k} = 0 \qquad (7.12)$$

by divide the above equation by $\frac{1}{\rho_s(1-\phi)}$ we will gain

-
$$\frac{1}{\rho_s}\frac{\partial \rho_s}{\partial t} + \frac{1}{(1 - \phi)}\frac{\partial (1 - \phi)}{\partial t} + \frac{\partial V_k^{(1)}}{\partial x_k} = 0 \qquad (7.13)$$

from the Equation of the state (EOS)

-
$$\frac{1}{\rho_s}\frac{\partial \rho_s}{\partial t} = \beta_s \frac{\partial P_f}{\partial t} \qquad (7.14)$$

also $\frac{\partial V_k^{(1)}}{\partial x_k}$ is the volumetric strain ε_v so the equation become

-
$$\frac{1}{(1 - \phi)}\frac{\partial (1 - \phi)}{\partial t} + \beta_s \frac{\partial P_f}{\partial t} + \frac{\partial V_k^{(1)}}{\partial x_k} = 0 \qquad (7.15)$$

by simplifying the above Eq

$$-\frac{1}{(1 - \phi)}\frac{\partial \phi}{\partial t} + \beta_s \frac{\partial P_f}{\partial t} + \frac{\partial V_k^{(1)}}{\partial x_k} \qquad (7.16)$$

also

$$d\phi = (1 - \phi)\left[\beta_s dp_f + \epsilon_v\right] \qquad (7.17)$$

by integrating the above equation :

$$\phi = \phi_o + (1 - \phi)\left[\phi_0 + \beta_s(p - p_o) + \epsilon_v\right] . \qquad (7.18)$$

and because we have a compression so the volumetric strain will be negative.

$$\phi = \phi_o + (1 - \phi)\left[\phi_0 + \beta_s(p - p_o) - \epsilon_v\right] . \qquad (7.19)$$

.A comparison of the numerical results against the analytical solution are shown in Fig. 7.8.

7.4. Benchmark 8 - THM

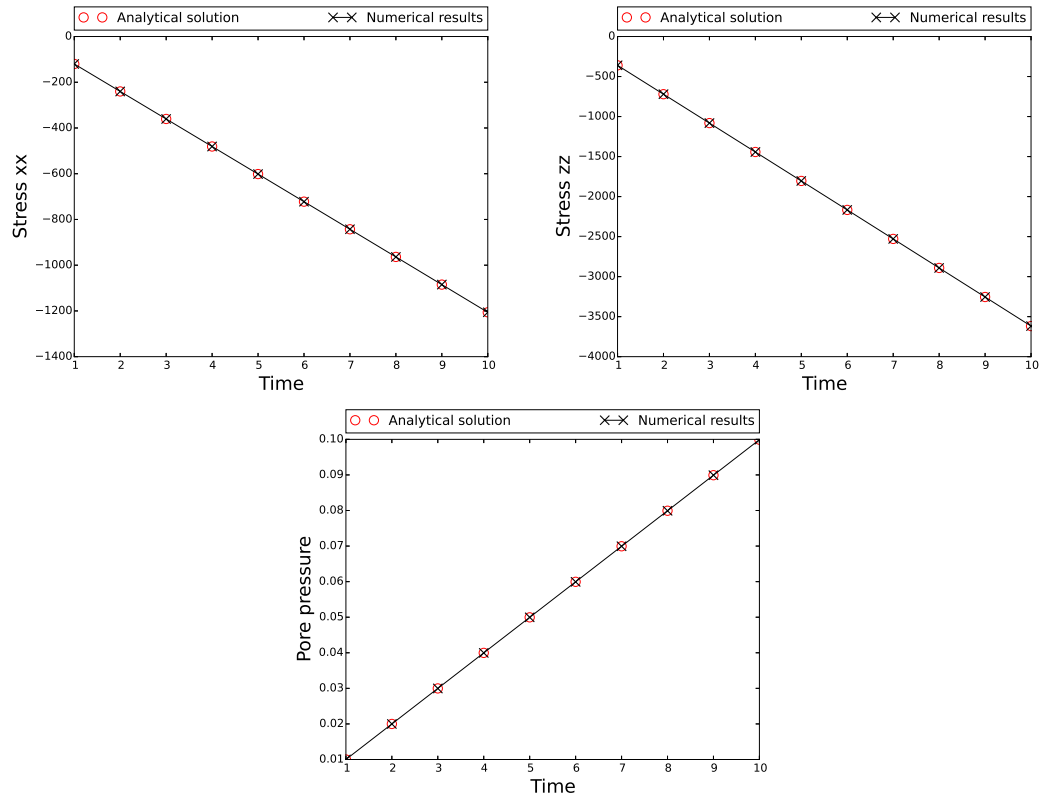Those benchmarks look at thermal-hydro-mechanical simulations.

Figure 7.8.: Comparison of analytical vs numerical results for benchmark 7.3.3

7.4.1. Analytical solution

The results are similar to those from Bench-HM elastic in Benchmark-7-HM and the stresses need to be augmented by a factor of thermal stress thermal stress is represented by this equation:

$$\sigma_t h = \beta \Delta T \tag{7.20}$$

where $\beta = \alpha \frac{E}{1-2\nu}$

so the stresses equation will become :

$$\sigma_{xx}^{\text{eff}} = \left[(K - \tfrac{2}{3}G) \left[(v_z t/L) + \left(\frac{1}{2} (v_z t/L)^2 \right) \right] \right] + \sigma_{th} . \tag{7.21}$$

$$\sigma_{zz}^{\text{eff}} = \left[(K + \tfrac{4}{3}G) \left[(v_z t/L) + \left(\frac{1}{2} (v_z t/L)^2 \right) \right] \right] + \sigma_{th} . \tag{7.22}$$

and the pore pressure equation will not change

$$P_{\text{f}} = -\frac{TimeFactor}{(1 - \phi)} (v_z t/L) \tag{7.23}$$

7.4.2. Numerical solution

This problem is then solved using moose on a generated 3D mesh for the values bellow:

- Young's modulus $(E) = 3.6$
- Poisson's ratio $(\nu) = 0.2$
- $\Phi = 0.1$
- $L = 1$
- Biot Coefficient $(\alpha) = 0.3$
- Péclet number $(Pe) = 10$
- solid compressibility $(\beta_s) = 3.7037$
- top velocity $(V_z) = 0.01$
- Thermal Coefficient Expansion $\alpha = 0.005$

A comparison of the numerical results against the analytical solution are shown in fig 7.10
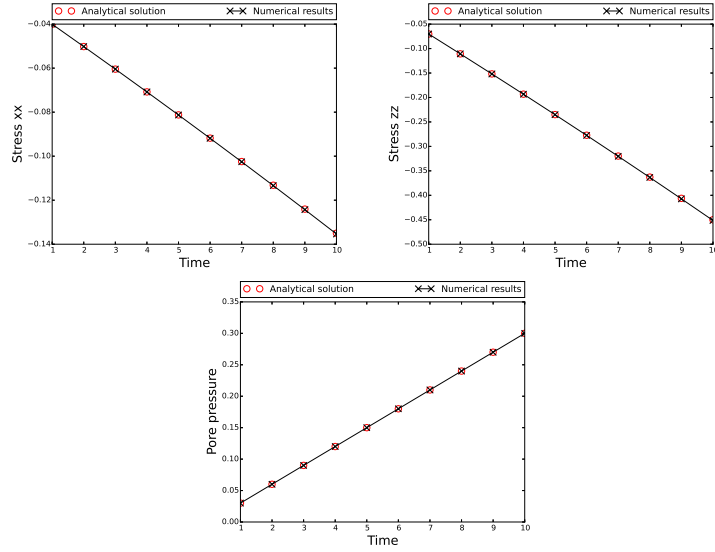
Figure 7.9.: Comparison of analytical vs numerical results for elastic with the effect of thermal stress for benchmark 7.4

7.5. Gravity

7.5.1. Gravity

7.5.1.1. Analytical Solution

Testing that gravity changes the stress (with depth for example) in the stress divergence kernel so the stress will be equal to the gravity and can be calculated from this equation

$$\sigma_{zz} = \rho g L \tag{7.24}$$

where:
ρ : solid density
g : gravitational acceleration
L : The length

$$\sigma_{xx} = K_o(\rho g L) \tag{7.25}$$

where: K_o :The ratio of horizontal to vertical stress

$$K_o = \frac{E\nu}{E(1-\nu)} \tag{7.26}$$

Lets explain the steps in details

$$K_o = \frac{\sigma_{xx}}{\sigma zz} \tag{7.27}$$

and

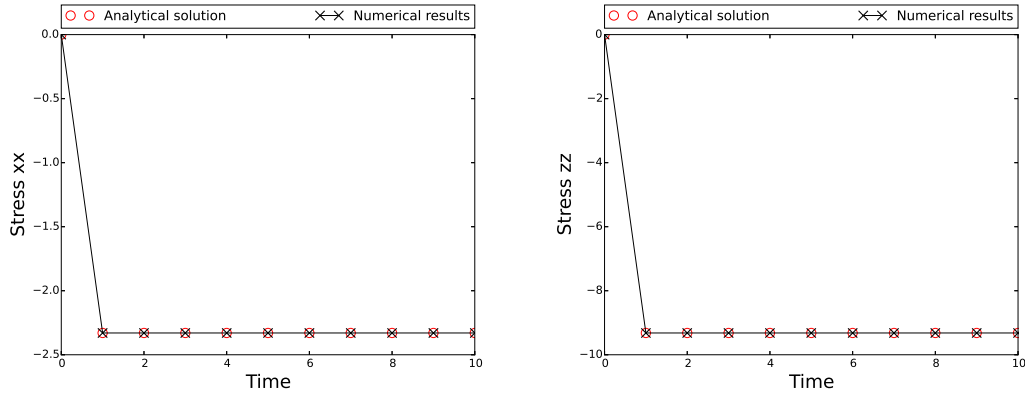$$K_o = \frac{(K - \frac{2}{3}G)\epsilon_{zz}}{(K + \frac{4}{3}G)\epsilon_{zz}} \tag{7.28}$$

31

Figure 7.10.: gravity $(\rho g h)$ changes the stress

when:

$$K = \frac{E}{3(1 - 2\nu)} \tag{7.29}$$

$$G = \frac{E}{2(1 + \nu)} \tag{7.30}$$

form more information about the two equation above see the table in this website: (https://en.wikipedia.org/wiki/Lamby substitute the two equations above in 7.28 and simplify them we end up with $K_o = \frac{E\nu}{E(1-\nu)}$

7.5.1.2. Numerical Solution

This problem is then solved using moose on a generated 3D mesh for the values bellow:

- Young's modulus $(E) = 5e4$

- gravitational acceleration $g = -9.81$

- Poisson's ratio $(\nu) = 0.2$

- $L = 1$

- solid density $(\rho = 1)$

a comparison of the numerical results against the analytical solution are shown in the figure 7.10

7.5.2. Gravity poro stress

7.5.2.1. Analytical Solution

Testing that gravity changes the stress (with depth for example) in the stress divergence kernel and taking into account pore pressure. The system is solved analytically as follows:

$$\sigma'_{zz} + p_f = \rho g h \tag{7.31}$$

32

$$p_f = -\frac{Pe}{(1-\phi)\beta}\frac{\sigma'_{zz}}{(k+\frac{4G}{3})} \tag{7.32}$$

$$\sigma'_{xx} = \sigma'_{yy} = K_0\sigma'_{zz} \tag{7.33}$$

and this gives the solution:

$$P_f = -\frac{Pe\rho gh}{\beta(1-\phi)k' - Pe} \tag{7.34}$$

where:
$k' = (K + \frac{4G}{3})$
lets explain the Eq. 7.34 in more details:
from Eq.7.31and 7.33 we get this equation

$$\sigma'_{zz} = \rho gh + \frac{Pe}{\beta(1-\phi)}\frac{\sigma'_{zz}}{(K+\frac{4G}{3})} \tag{7.35}$$

by rearrange the equation above we end up with

$$\sigma'_{zz} - \frac{Pe}{\beta(1-\phi)}\frac{\sigma'_{zz}}{(K+\frac{4G}{3})} = \rho gh \tag{7.36}$$

by simplifying more

$$\sigma'_{zz}\left(1 - \frac{Pe}{\beta(1-\phi)k'}\right) = \rho gh \tag{7.37}$$

and

$$\sigma'_{zz} = \frac{\rho gh}{\left(1 - \frac{Pe}{\beta(1-\phi)k'}\right)} \tag{7.38}$$

by multiply the equation above by $\frac{\beta(1-\phi)K'}{\beta(1-\phi)K'}$ we end up with

$$\sigma'_{zz} = \frac{(\rho gh)\beta(1-\phi)K'}{\beta(1-\phi)K' - Pe} \tag{7.39}$$

by substitute the above equation in Eq.7.33 we get the Eq. 7.34

7.5.2.2. Numerical Solution

This problem is then solved using moose on a generated 3D mesh for the values bellow:

- Young's modulus $(E) = 5e4$

- gravitational acceleration $g = -9.81$

- Poisson's ratio $(\nu) = 0.2$

- $L = 1$

- solid density $(\rho = 1)$
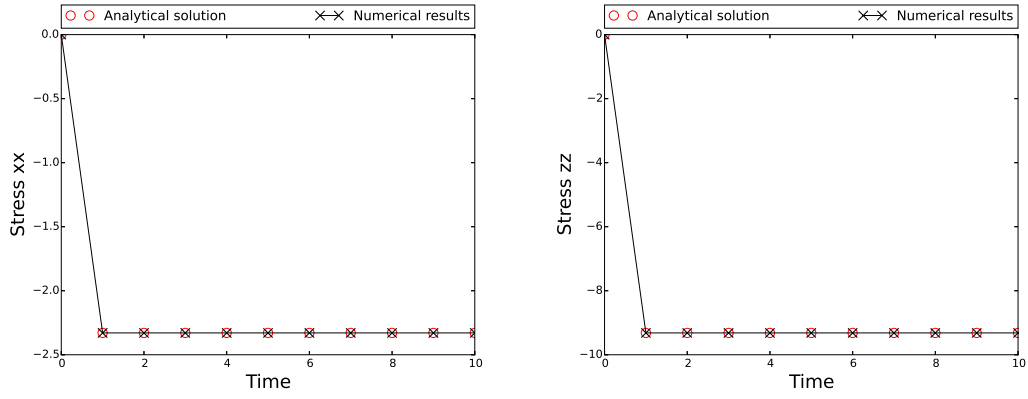
Figure 7.11.: a comparison of the numerical results against the analytical solution are shown in the figure 7.10 gravity changes the stress and taking into account pore pressure.

- solid compressibility $\beta = 1.111111$

- Péclet number $(Pe) = 10$

- $K = 27,777.8$

- $G = 20,833.333$

a comparison of the numerical results against the analytical solution are shown in the figure7.11

A. Derivations

This chapter documents some of the derivations used to obtain the equations presented in Sec.2.

A.1. Mass balance

We define the following densities

$$\rho_1 = (1 - \phi)\rho_s \tag{A.1a}$$

$$\rho_2 = \phi\,\rho_f \tag{A.1b}$$

and we use the usual material derivative definition

$$\frac{D^{(i)}.}{Dt} = \frac{\partial.}{\partial t} + v_k^{(i)}\frac{\partial.}{\partial x_k} \tag{A.2}$$

Mass balance for the fluid phase

$$\frac{\partial \rho_2}{\partial t} + \frac{\partial(\rho_2 V_k^{(2)})}{\partial x_k} = j_1 \tag{A.3}$$

Using Eq. A.1b in Eq. A.3 we get

$$\phi\frac{\partial \rho_f}{\partial t} + \rho_f\frac{\partial \phi}{\partial t} + \rho_f\frac{\partial(\phi V_k^{(2)})}{\partial x_k} + \phi V_k^{(2)}\frac{\partial \rho_f}{\partial x_k} = j_1 \tag{A.4}$$

Dividing by ρ_f we obtain

$$\frac{\phi}{\rho_f}\frac{D^{(2)}\rho_f}{Dt} + \frac{\partial \phi}{\partial t} + \frac{\partial(\phi V_k^{(2)})}{\partial x_k} = \frac{j_1}{\rho_f} \tag{A.5}$$

Mass balance for the solid phase

$$\frac{\partial \rho_1}{\partial t} + \frac{\partial(\rho_1 V_k^{(1)})}{\partial x_k} = -j_1 \tag{A.6}$$

Using Eq. A.1a in Eq. A.6 we get

$$(1 - \phi)\frac{\partial \rho_s}{\partial t} - \rho_s\frac{\partial \phi}{\partial t} + \rho_s\frac{\partial((1 - \phi)V_k^{(1)})}{\partial x_k} + (1 - \phi)V_k^{(1)}\frac{\partial \rho_s}{\partial x_k} = -j_1 \tag{A.7}$$

Dividing by ρ_s we obtain

$$\frac{(1-\phi)}{\rho_s}\frac{D^{(1)}\rho_s}{Dt} - \frac{\partial\phi}{\partial t} + \frac{\partial(V_k^{(1)})}{\partial x_k} - \frac{\partial(\phi V_k^{(1)})}{\partial x_k} = -\frac{j_1}{\rho_s} \tag{A.8}$$

Mass balance for the mixture (solid + fluid)
Adding Eq. A.5 and Eq. A.8 gives the mixture mass balance:

$$\frac{(1-\phi)}{\rho_s}\frac{D^{(1)}\rho_s}{Dt} + \frac{\phi}{\rho_f}\frac{D^{(2)}\rho_f}{Dt} + \frac{\partial(\phi(V_k^{(2)}-V_k^{(1)}))}{\partial x_k} + \frac{\partial(V_k^{(1)})}{\partial x_k} = \left(\frac{1}{\rho_f}-\frac{1}{\rho_s}\right)j_1 \tag{A.9}$$

Equation of state (EOS)

$$\frac{d\rho_{(i)}}{\rho_{(i)}} = \left(\frac{d\rho_{(i)}}{dp_f}\right)_T \frac{dp_f}{\rho_{(i)}} + \left(\frac{d\rho_{(i)}}{dT}\right)_p \frac{dT}{\rho_{(i)}}, \quad i \in \{s,f\} \tag{A.10}$$

Using the definition for compressibility $\beta_{(i)} = \frac{1}{\rho_{(i)}}\left(\frac{d\rho_{(i)}}{dp_f}\right)_T$ and thermal expansion $\lambda_{(i)} = -\frac{1}{\rho_{(i)}}\left(\frac{d\rho_{(i)}}{dT}\right)_{p_f}$ we get the Equation of State (EOS)

$$\frac{d\rho_{(i)}}{\rho_{(i)}} = \beta_{(i)}dp_f - \lambda_{(i)}dT, \quad i \in \{s,f\} \tag{A.11}$$

Using Eq. A.11 in Eq. A.9 leads to

$$(1-\phi)\left[\beta_s\frac{D^{(1)}p_f}{Dt} - \lambda_s\frac{D^{(1)}T}{Dt}\right] + \phi\left[\beta_f\frac{D^{(2)}p_f}{Dt} - \lambda_f\frac{D^{(2)}T}{Dt}\right]$$
$$+ \frac{\partial(\phi(V_k^{(2)}-V_k^{(1)}))}{\partial x_k} + \frac{\partial(V_k^{(1)})}{\partial x_k} = \left(\frac{1}{\rho_f}-\frac{1}{\rho_s}\right)j_1 \tag{A.12}$$

Rearranging the terms we get

$$\overbrace{[(1-\phi)\beta_s + \phi\beta_f]}^{\beta_m}\frac{\partial p_f}{\partial t} - \overbrace{[(1-\phi)\lambda_s + \phi\lambda_f]}^{\lambda_m}\frac{\partial T}{\partial t}$$
$$+ \left[(1-\phi)\beta_s V_k^{(1)} + \phi\beta_f V_k^{(2)}\right]\frac{\partial p_f}{\partial x_k} - \left[(1-\phi)\lambda_s V_k^{(1)} + \phi\lambda_f V_k^{(2)}\right]\frac{\partial T}{\partial x_k}$$
$$+ \frac{\partial(\phi(V_k^{(2)}-V_k^{(1)}))}{\partial x_k} + \frac{\partial(V_k^{(1)})}{\partial x_k} = \left(\frac{1}{\rho_f}-\frac{1}{\rho_s}\right)j_1 \tag{A.13}$$

Normalisation

In order to deal with dimensionless parameters we introduce the following normalised variables

$$p^* = \frac{p_f}{\sigma_{ref}}, \tag{A.14a}$$

$$T^* = \frac{T - T_{ref}}{\delta T_{ref}}, \tag{A.14b}$$

$$x^* = \frac{x}{x_{ref}}, \tag{A.14c}$$

$$t^* = \frac{c_{th}}{x_{ref}^2}t, \tag{A.14d}$$

$$V^* = \frac{V}{V_{ref}}. \tag{A.14e}$$

where $c_{th} = \alpha/(\rho C_p)_m$ is the thermal diffusivity of the mixture. Dividing Eq. A.13 by β_m and switching to the normalised variables we get

$$\frac{\sigma_{ref}\, c_{th}}{x_{ref}^2} \frac{\partial p^*}{\partial t^*} - \frac{\lambda_m\, \delta\, T_{ref}\, c_{th}}{\beta_m\, x_{ref}^2} \frac{\partial T^*}{\partial t^*}$$

$$+ \frac{V_{ref}\, \sigma_{ref}}{x_{ref}} \left[\frac{(1-\phi)\beta_s V_k^{*(1)} + \phi\beta_f V_k^{*(2)}}{\beta_m} \right] \frac{\partial p^*}{\partial x_k^*}$$

$$- \frac{V_{ref}\, \delta\, T_{ref}}{x_{ref}} \left[\frac{(1-\phi)\lambda_s V_k^{*(1)} + \phi\lambda_f V_k^{*(2)}}{\beta_m} \right] \frac{\partial T*}{\partial x_k^*}$$

$$+ \frac{V_{ref}}{\beta_m\, x_{ref}} \frac{\partial(\phi(V_k^{*(2)} - V_k^{*(1)}))}{\partial x_k^*} + \frac{V_{ref}}{\beta_m\, x_{ref}} \frac{\partial(V_k^{*(1)})}{\partial x_k^*} = \frac{1}{\beta_m}\left(\frac{1}{\rho_f} - \frac{1}{\rho_s}\right)j_1 \quad (A.15)$$

This can be rewritten as

$$\frac{\partial p^*}{\partial t^*} - \overbrace{\frac{\lambda_m\, \delta\, T_{ref}}{\beta_m\, \sigma_{ref}}}^{\Lambda} \frac{\partial T^*}{\partial t^*} + \overbrace{\frac{x_{ref}\, V_{ref}}{c_{th}}}^{Pe} \overbrace{\left[\frac{(1-\phi)(\sigma_{ref}\beta_s)V_k^{*(1)} + \phi(\sigma_{ref}\beta_f)V_k^{*(2)}}{\sigma_{ref}\beta_m} \right]}^{\vec{v}^p} \frac{\partial p^*}{\partial x_k^*}$$

$$- \overbrace{\frac{x_{ref}\, V_{ref}}{c_{th}}}^{Pe} \overbrace{\left[\frac{(1-\phi)(\delta\, T_{ref}\lambda_s)V_k^{*(1)} + \phi(\delta\, T_{ref}\lambda_f)V_k^{*(2)}}{\sigma_{ref}\beta_m} \right]}^{\vec{v}^T} \frac{\partial T*}{\partial x_k^*}$$

$$+ \frac{x_{ref}\, V_{ref}}{c_{th}\, \beta_m\, \sigma_{ref}} \frac{\partial}{\partial x_k^*} \underbrace{\left[\phi(V_k^{*(2)} - V_k^{*(1)}) \right]}_{\text{norm. filtration vec.}} + \underbrace{\frac{x_{ref}\, V_{ref}}{c_{th}}}_{Pe} \frac{1}{\beta_m\, \sigma_{ref}} \underbrace{\frac{\partial(V_k^{*(1)})}{\partial x_k^*}}_{\dot{\epsilon}_V^*}$$

$$= \frac{x_{ref}^2}{\beta_m\, \sigma_{ref}\, c_{th}}\left(\frac{1}{\rho_f} - \frac{1}{\rho_s}\right)j_1 \quad (A.16)$$

37

with

$$\Lambda = \frac{\lambda_m \, \delta \, T_{ref}}{\beta_m \, \sigma_{ref}} = \frac{\lambda_m^*}{\beta_m^*}, \tag{A.17a}$$

$$\lambda_i^* = \delta \, T_{ref} \, \lambda_i, \quad i \in \{s, f, m\} \tag{A.17b}$$

$$\beta_i^* = \beta \, \sigma_{ref}, \quad i \in \{s, f, m\} \tag{A.17c}$$

$$Pe = \frac{x_{ref} \, V_{ref}}{c_{th}}, \tag{A.17d}$$

$$v^p = \frac{(1-\phi)\beta_s^* V_k^{*(1)} + \phi\beta_f^* V_k^{*(2)}}{\beta_m^*}, \tag{A.17e}$$

$$v^T = \frac{(1-\phi)\lambda_s^* V_k^{*(1)} + \phi\lambda_f^* V_k^{*(2)}}{\beta_m^*}. \tag{A.17f}$$

The filtration vector $\phi(V_k^{(2)} - V_k^{(1)})$ can be expressed using Darcy's law as

$$\phi(V_k^{(2)} - V_k^{(1)}) = -\frac{\kappa}{\mu_f} \left(\frac{\partial p_f}{\partial x_k} - \rho_f \, g \, \vec{e}_z \right) \tag{A.18}$$

In its normalised form it becomes

$$\phi(V_k^{*(2)} - V_k^{*(1)}) = -\frac{\kappa}{\mu_f} \frac{\sigma_{ref}}{x_{ref} \, V_{ref}} \left(\frac{\partial p^*}{\partial x_k^*} - \frac{x_{ref}}{\sigma_{ref}} \rho_f \, g \, \vec{e}_z \right) \tag{A.19}$$

The mass balance equation then becomes

$$\frac{\partial p^*}{\partial t^*} - \Lambda \frac{\partial T^*}{\partial t^*} + Pe \, \vec{v}^p \frac{\partial p^*}{\partial x_k^*} - Pe \, \vec{v}^T \frac{\partial T*}{\partial x_k^*}$$

$$+ \frac{\partial}{\partial x_k^*} \left[\underbrace{\frac{\kappa \, \sigma_{ref}}{\mu_f \, c_{th} \, \beta_m^*}}_{1/Le} \left(\frac{\partial p^*}{\partial x_k^*} - \underbrace{\rho_f \frac{x_{ref}}{\sigma_{ref}} g}_{(\rho_f \, g)^*} \, \vec{e}_z \right) \right] + \frac{Pe}{\beta_m^*} \dot{\epsilon}_V^* = \frac{x_{ref}^2}{\beta_m \, \sigma_{ref} \, c_{th}} \left(\frac{1}{\rho_f} - \frac{1}{\rho_s} \right) j_1$$

$$\tag{A.20}$$

with the Lewis number defined as $Le = \frac{\mu_f \, c_{th} \, \beta_m^*}{\kappa \, \sigma_{ref}}$ and the normalised gravity term $(\rho_f \, g)^* = \rho_f \frac{x_{ref}}{\sigma_{ref}} g$.

Following (Alevizos et al., 2014, appendix A) $j_1 = \omega_F . M_B$, $\omega_F = \frac{\rho_1}{M_{AB}} k_F exp - \Delta H_{act}^F / RT$ and $\rho_1 = (1-\phi)(1-s)\rho_{AB}$, so the volumetric source term j_1 can be written as

$$j_1 = \rho_{AB} \frac{M_B}{M_{AB}} (1-\phi)(1-s) k_F exp(-\Delta H_{act}^F / RT) \tag{A.21}$$

The RHS term of Eq. A.20 can then be written as

$$\frac{x_{ref}^2}{\beta_m\,\sigma_{ref}\,c_{th}}\left(\frac{1}{\rho_f}-\frac{1}{\rho_s}\right)j_1 = \frac{x_{ref}^2}{\beta_m\,\sigma_{ref}\,c_{th}}\left(\frac{1}{\rho_f}-\frac{1}{\rho_s}\right)\rho_{AB}\frac{M_B}{M_{AB}}(1-\phi)(1-s)k_F exp(-\Delta H_{act}^F/RT)$$

$$= \underbrace{\frac{x_{ref}^2 k_F}{\beta_m\,\sigma_{ref}\,c_{th}}\frac{\rho_{AB}}{\rho_B}\frac{M_B}{M_{AB}}\left(\frac{\rho_B}{\rho_f}-\frac{\rho_B}{\rho_s}\right)e^{-Ar_F}}_{1/Le_{chem}}\underbrace{(1-\phi)(1-s)\exp\left(\frac{Ar_F\,\delta T^*}{1+\delta T^*}\right)}_{\omega_F^*} \quad (A.22)$$

We then arrive to the full mass balance equation Eq. 2.1b

A.2. Energy balance

The local form of the energy balance equation reads as follows:

$$(\rho C_p)_m\frac{D^{(m)}T}{Dt} = \alpha\nabla^2 T + \chi\sigma_{ij}.\dot{\epsilon}_{ij}^p - \Delta H(\omega_F - \omega_R) \quad (A.23)$$

with χ the Taylor-Quinney coefficient and $\Delta H_r = \Delta\mathfrak{E} = \mathfrak{E}_F - \mathfrak{E}_R$ the reaction's specific enthalpy. The definitions of the reaction rates ω_F and ω_R are (from Eq. 2.7)

$$\omega_F = k_F(1-s)(1-\phi)\frac{\rho_{AB}}{M_{AB}}e^{-\Delta H_{act}^F/RT} \quad (A.24a)$$

$$\omega_R = k_R\,s(1-\phi)\Delta\phi_{chem}\frac{\rho_A\rho_B}{\rho_{AB}}\frac{M_{AB}}{M_A M_B}e^{-\Delta H_{act}^R/RT} \quad (A.24b)$$

Using the normalised variable we get

$$\frac{\delta T_{ref}\,c_{th}}{x_{ref}^2}(\rho C_p)_m\frac{\partial T^*}{\partial t^*} + \frac{\delta T_{ref}\,v_{ref}}{x_{ref}}(\rho C_p)_m\,\bar{v}\,\frac{\partial T^*}{\partial x^*}$$

$$-\frac{\alpha\,\delta T_{ref}}{x_{ref}^2}\nabla^2 T - \frac{\sigma_{ref}\,c_{th}}{x_{ref}^2}\chi\sigma_{ij}^*\,\dot{\epsilon}_{ij}^{*(p)}$$

$$-\Delta H_r\,k_F(1-s)(1-\phi)\frac{\rho_{AB}}{M_{AB}}e^{-\Delta H_{act}^F/RT}$$

$$+\Delta H_r\,k_R\,s(1-\phi)\Delta\phi_{chem}\frac{\rho_A\rho_B}{\rho_{AB}}\frac{M_{AB}}{M_A M_B}e^{-\Delta H_{act}^R/RT} = 0 \quad (A.25)$$

Note that the reference strain rate is also rescaled so

$$\dot{\epsilon}_0^* = \dot{\epsilon}_0\frac{x_{ref}^2}{c_{th}} \quad (A.26)$$

This leads to

$$
\frac{\partial T^*}{\partial t^*} + \overbrace{\frac{x_{ref}\, v_{ref}}{c_{th}}}^{Pe} \bar{v}\, \frac{\partial T^*}{\partial x^*} - \overbrace{\frac{\alpha}{(\rho C_p)_m}}^{c_{th}} \frac{1}{c_{th}} \nabla^2 T - \overbrace{\frac{\sigma_{ref}}{\delta T_{ref}(\rho C_p)_m}}^{Gr} \chi\, \sigma_{ij}^*\, \dot{\epsilon}_{ij}^{*(p)}
$$

$$
- \underbrace{\frac{\Delta H_r\, x_{ref}^2 k_F}{\delta T_{ref}\, \alpha} \frac{\rho_{AB}}{M_{AB}} e^{-Ar_F}}_{Da_{endo}} (1-s)(1-\phi) e^{\frac{Ar_F\, \delta T^*}{1+\delta T^*}}
$$

$$
+ \underbrace{\frac{\Delta H_r\, x_{ref}^2 k_R}{\delta T_{ref}\alpha} \frac{\rho_A \rho_B}{\rho_{AB}} \frac{M_{AB}}{M_A M_B} e^{-Ar_R}}_{Da_{exo}} s(1-\phi)\Delta\phi_{chem} e^{\frac{Ar_R\, \delta T^*}{1+\delta T^*}} = 0 \quad \text{(A.27)}
$$

and finally to Eq. 2.1c

A.3. Jacobians

Numerical convergence can be helped by providing the jacobians and off-diagonal terms for the kernel residuals, even though MOOSE does not explicitly require them. It is a trial-and-error process to check if the improvement in convergence justifies the cost of computing those terms. See the MOOSE workshop manual on `http://mooseframework.org/documentation/` for more details.

If $R(u)$ is the residual for the variable u, the jacobian matrix J is defined as

$$
J_{ij}(u) = \frac{\partial R_i(u)}{\partial u_j} \quad \text{(A.28)}
$$

and the off-diagonal jacobian term for another coupled variable v as

$$
J_{ij}^{(\text{off diag})}(u) = \frac{\partial R_i(u)}{\partial v_j} \quad \text{(A.29)}
$$

A.3.1. RedbackMassConvection

The residual is defined as

$$
R = Pe\, v^p.\nabla p^* - Pe\, v^T.\nabla T^* \quad \text{(A.30)}
$$

with (see Eq.2.1)

$$
v_i^p = (1-\phi)\frac{\beta_s^*}{\beta_m^*} v_i^{*(s)} + \phi\frac{\beta_f^*}{\beta_m^*} v_i^{*(f)},
$$

$$
v_i^T = (1-\phi)\frac{\lambda_s^*}{\beta_m^*} v_i^{*(s)} + \phi\frac{\lambda_f^*}{\beta_m^*} v_i^{*(f)}.
$$

Noting that $\frac{\partial \nabla u}{\partial u_j} = \nabla \phi_j$ for any variable u (see MOOSE documentation),

$$J = \frac{\partial R}{\partial p^*} = Pe \frac{\partial v^p}{\partial p^*} . \nabla p^* + Pe \, v^p \, \nabla \phi_j - Pe \frac{\partial v^T}{\partial p^*} . \nabla T^* \qquad \text{(A.31)}$$

The normalised filtration vector (Eq. A.19) can be rewritten as

$$\phi(v^{*(f)} - v^{*(s)}) = -\frac{\beta_m^*}{Le \, Pe} \left(\nabla p^* - \rho_f \, g^* \right) \qquad \text{(A.32)}$$

Deriving that equation and adding the equation of state (Eq. A.11) we get

$$\frac{\partial(\phi v^{*(f)})}{\partial p^*} = -\frac{\beta_m^*}{Le \, Pe} \left(\nabla \phi_j - \beta_f^* \rho_f \, g^* \right) \qquad \text{(A.33)}$$

under the following simplifying assumptions:

- $\frac{\partial v^{(s)}}{\partial p^*} = 0$

- $\frac{\partial \mu_f}{\partial p^*} = 0$

- $\frac{\partial \phi}{\partial p^*} = 0$

Using $\frac{\partial \rho_f}{\partial p^*} = \beta_f^* \, \rho_f$ we get

$$\frac{\partial v^p}{\partial p^*} = -\frac{\beta_f^*}{Le \, Pe} \left(\nabla \phi_j - \beta_f^* \rho_f \, g^* \right) \qquad \text{(A.34a)}$$

$$\frac{\partial v^T}{\partial p^*} = -\frac{\lambda_f^*}{Le \, Pe} \left(\nabla \phi_j - \beta_f^* \rho_f \, g^* \right) \qquad \text{(A.34b)}$$

Eq. A.31 then becomes

$$J = Pe \frac{\partial v^p}{\partial p^*} . \nabla p^* + Pe \, v^p \, \nabla \phi_j - Pe \frac{\partial v^T}{\partial p^*} . \nabla T^* \qquad \text{(A.35a)}$$

$$= -\frac{1}{Le} \left(\nabla \phi_j - \beta_f^* \rho_f \, g^* \right) \left(\beta_f^* \nabla p^* - \lambda_f^* \nabla T^* \right) + Pe \, v^p \, \nabla \phi_j$$

$$= \left(Pe \, v^p - \frac{1}{Le}(\beta_f^* \nabla p^* - \lambda_f^* \nabla T^*) \right) \nabla \phi_j + \frac{1}{Le} \beta_f^* \rho_f \, g^* (\beta_f^* \nabla p^* - \lambda_f^* \nabla T^*)$$

Using $\frac{\partial \rho_f}{\partial T^*} = -\lambda_f^* \, \rho_f$ we get

$$\frac{\partial v^p}{\partial T^*} = -\frac{\beta_f^* \lambda_f^*}{Le \, Pe} \rho_f \, g^* \qquad \text{(A.36a)}$$

$$\frac{\partial v^T}{\partial T^*} = -\frac{\lambda_f^{*2}}{Le \, Pe} \rho_f \, g^* \qquad \text{(A.36b)}$$

$$\text{(A.36c)}$$

The off-diagonal jacobian with respect to temperature is defined as

$$J^T = \frac{\partial R}{\partial T^*} = Pe \frac{\partial v^p}{\partial T^*}.\nabla p^* - Pe \frac{\partial v^T}{\partial T^*}\nabla T* - Pe\, v^T \nabla \phi_j \tag{A.37a}$$

$$= -\frac{\lambda_f^*}{Le}\rho_f\, g^*(\beta_f^*\nabla p^* - \lambda_f^*\nabla T*) - Pe\, v^T \nabla \phi_j$$

A.3.2. RedbackThermalConvection

The residual is defined as

$$R = Pe\, \bar{v}.\nabla T^* \tag{A.38}$$

and the corresponding jacobian as

$$J = \frac{\partial R}{\partial T^*} = Pe \frac{\partial \bar{v}}{\partial T^*}.\nabla T^* + Pe\, \bar{v}\, \nabla \phi_j. \tag{A.39}$$

From the definition of the normalised filtration velocity (Eq. A.32) we get

$$\frac{\partial v^{*(f)}}{\partial T^*} = -\frac{\beta_m^* \lambda_f^*}{Le\, Pe\, \phi}\rho_f\, g^* \tag{A.40}$$

From the definition of the mixture barycentric velocity $\bar{v} = \frac{\rho_s}{\rho}v^{*(s)} + \frac{\rho_f}{\rho}v^{*(f)}$ and following the same assumptions that led to Eq. A.34 we write

$$\frac{\partial \bar{v}}{\partial T^*} = -\frac{1}{\bar{\rho}^2}\frac{\partial \bar{\rho}}{\partial T^*}(\rho_s v^{*(s)} + \rho_f v^{*(f)}) + \frac{1}{\bar{\rho}}\left[\frac{\partial \rho_s}{\partial T^*}v^{*(s)} + \frac{\partial \rho_f}{\partial T^*}v^{*(f)} + \rho_f \frac{\partial v^{*(f)}}{\partial T^*}\right] \tag{A.41a}$$

$$= -\frac{1}{\bar{\rho}}\frac{\partial \bar{\rho}}{\partial T^*}\bar{v} + \frac{1}{\bar{\rho}}\left[\frac{\partial \rho_s}{\partial T^*}v^{*(s)} + \frac{\partial \rho_f}{\partial T^*}v^{*(f)} + \rho_f \frac{\partial v^{*(f)}}{\partial T^*}\right]$$

$$= \frac{1}{\bar{\rho}}\left[(1-\phi)\lambda^{*(s)}\rho_s + \phi\lambda^{*(f)}\rho_s\right]\bar{v} - \frac{1}{\bar{\rho}}\left[\lambda^{*(s)}\rho_s v^{*(s)} + \lambda^{*(f)}\rho_f v^{*(f)}\right] - \frac{\rho_f}{\bar{\rho}}\frac{\beta_m^* \lambda_f^*}{Le\, Pe\, \phi}\rho_f\, g^*$$

$$= ...$$

$$= \frac{1}{\bar{\rho}}\left[\lambda_m^*\rho_s\bar{v} - \lambda_s^*\rho_s v^{*(s)} - \lambda_f^*\rho_f v^{*(f)}\right] - \frac{\rho_f}{\bar{\rho}}\frac{\beta_m^* \lambda_f^*}{Le\, Pe\, \phi}\rho_f\, g^*$$

For the off-diagonal term with respect to pore pressure we get

$$\frac{\partial \bar{v}}{\partial p^*} = -\frac{1}{\bar{\rho}^2}\frac{\partial \bar{\rho}}{\partial p^*}(\rho_s v^{*(s)} + \rho_f v^{*(f)}) + \frac{1}{\bar{\rho}}\left[\frac{\partial \rho_s}{\partial p^*}v^{*(s)} + \frac{\partial \rho_f}{\partial p^*}v^{*(f)} + \rho_f \frac{\partial v^{*(f)}}{\partial p^*}\right] \quad \text{(A.42a)}$$

$$= -\frac{1}{\bar{\rho}}\frac{\partial \bar{\rho}}{\partial p^*}\bar{v} + \frac{1}{\bar{\rho}}\left[\frac{\partial \rho_s}{\partial p^*}v^{*(s)} + \frac{\partial \rho_f}{\partial p^*}v^{*(f)} + \rho_f \frac{\partial v^{*(f)}}{\partial p^*}\right]$$

$$= -\frac{1}{\bar{\rho}}\left[(1-\phi)\beta^{*(s)}\rho_s + \phi\beta^{*(f)}\rho_s\right]\bar{v} + \frac{1}{\bar{\rho}}\left[\beta^{*(s)}\rho_s v^{*(s)} + \beta^{*(f)}\rho_f v^{*(f)}\right]$$

$$\quad - \frac{\rho_f}{\bar{\rho}}\frac{\beta_m^*}{Le\,Pe\,\phi}\left(\nabla \phi_j - \beta_f^* \rho_f\, g^*\right)$$

$$=\ldots$$

$$= \frac{1}{\bar{\rho}}\left[-\beta_m^*\rho_s\bar{v} + \beta_s^*\rho_s v^{*(s)} + \beta_f^*\rho_f v^{*(f)}\right] - \frac{\rho_f}{\bar{\rho}}\frac{\beta_m^*}{Le\,Pe\,\phi}\left(\nabla \phi_j - \beta_f^* \rho_f\, g^*\right)$$

B. Symbols

Tab. B.1 lists some of the main symbols used in this document.

Table B.1.: List of main symbols

Symbol	Name	Unit of measure
Ar	Arrhenius number	-
Ar_F	Forward Arrhenius number	-
Ar_R	Reverse Arrhenius number	-
Da_{endo}	Endothermic Damköhler number	-
Da_{exo}	Exothermic Damköhler number	-
Gr	Gruntfest number	-
$\bar{\Lambda}$	Thermal pressurization coefficient	-
Le	Lewis number	-
Le_{chem}	Chemical Lewis number	-
Pe	Péclet number	-
$.^{\star}, [t^{\star}, x^{\star}, T^{\star}, \Delta p^{\star}, \sigma_{ij}^{\star}]$	Normalized variables [time, space, temperature, pore pressure increase, stress]	-
α	Thermal conductivity	$kg.m.K^{-1}.s^{-3}$
$\beta, [\beta_s, \beta_f]$	Compressibility [solid, fluid phase]	Pa^{-1}
δ	Numerical rescaling parameter	-
δ_{ij}	Kronecker delta	-
$\Delta H, [\Delta H_r, \Delta H_{act}^F, \Delta H_{act}^R, \Delta H_{mech}]$	Change of specific enthalpy [enthalpy of reaction, activation enthalpy of forward, reverse reaction]	$J.mol^{-1}$
ϵ_{ij}	Strain tensor	-
$\dot{\epsilon}_{ij}$	Strain rate tensor	s^{-1}
$\dot{\epsilon}, [\dot{\epsilon}_0, \dot{\epsilon}_d^{vp}, \dot{\epsilon}_v^{vp}]$	Strain rate [reference, deviatoric visco-plastic, volumetric visco-plastic]	s^{-1}
$\zeta, [\zeta_1, \zeta_2, \zeta_3]$	Stoichiometric coefficients [of species AB, A, B] from Eq. 2.4	-
κ	Permeability	m^2
$\lambda, [\lambda_s, \lambda_f]$	Thermal expansion coefficient [solid, fluid phase]	K^{-1}
μ_f	Fluid viscosity	$Pa.s$
ν	Poisson's ratio	-
$\dot{\Pi}$	Plastic multiplier (scalar)	s^{-1}
$\rho, [\rho_{AB}, \rho_A, \rho_B, \rho_s, \rho_f, \rho_1, \rho_2]$	Density [of species AB, A, B, solid, fluid, solid phase, fluid phase]	$kg.m^{-3}$
$\sigma_{ij}, [\sigma_{ij}']$	Stress tensor [effective stress]	Pa
$\phi, [\phi_0, \Delta\phi_{chem}, \Delta\phi_{mech}]$	Porosity [initial, chemical component, mechanical component]	-
χ	Taylor-Quinney coefficient	-
$\omega, [\omega_{AB}, \omega_A, \omega_B, \omega_F, \omega_R]$	Molar reaction rates [of species AB, A, B, forward, reverse]	$mol.m^{-3}.s^{-1}$
A_ϕ	Interconnected porosity coefficient	-
C_{ijkl}^e	Elasticity tensor	Pa

Symbol	Name	Unit of measure
	B.1 – continued from previous page	
C_p	Specific heat capacity	$m^2.K^{-1}.s^{-2}$
E	Young's modulus	Pa
$\mathfrak{E}$	Activation energy	$J.mol^{-1}$
G	Shear modulus	Pa
K	Bulk modulus	Pa
K_c	Relative pre-exponential factor	-
$M, [M_{AB}, M_A, M_B]$	Molar mass [of species AB, A, B]	$kg.mol^{-1}$
R	Universal gas constant	$J.K^{-1}.mol^{-1}$
T	Temperature	K
$V, [V_s, V_f, V_A, V_B,$ $V_{AB}, V_{act}]$	Volume [of solid phase, fluid phase, component A, B, AB, activation volume]	m^3
b_i	Body force vector	$m^2.s^{-1}$
c_{th}	Thermal diffusivity	$m^2.s^{-1}$
$j, [j_1, j_2]$	Mass production rate per unit volume [solid, fluid phase]	$kg.m^{-3}.s^{-1}$
$k, [k_F, k_R, k_A, k_B]$	Pre-exponential factor [of forward, reverse chemical reaction, for species A, B]	s^{-1}
m	Visco-plasticity power law exponent	-
$p, [p_Y]$	Volumetric mean stress [value at yield]	Pa
p_f	Pore fluid pressure	Pa
$q, [q_Y]$	Equivalent stress [value at yield]	Pa
f	Yield function	$\mathbb{R}^9 \longrightarrow \mathbb{R}$
s	partial solid ratio	-
$v_i, [v_i^s, v_i^f, \bar{v}_i^m, \bar{v}_i^\beta, \bar{v}_i^\Lambda]$	Velocity vector [solid, fluid phase, average velocity of the mixture with respect to mass (barycentric), compressibility, thermal pressurisation]	$m.s^{-1}$

Bibliography

S. Alevizos, T. Poulet, E. Veveakis, Thermo-poro-mechanics of chemically active creeping faults. 1: Theory and steady state considerations. Journal of Geophysical Research: Solid Earth **119**(6), 4558–4582 (2014). doi:10.1002/2013JB010070

N. Austin, B. Evans, The kinetics of microstructural evolution during deformation of calcite. Journal of Geophysical Research: Solid Earth **114**(B9), (2009). B09402. doi:10.1029/2008JB006138. http://dx.doi.org/10.1029/2008JB006138

N.J. Austin, B. Evans, Paleowattmeters: A scaling relation for dynamically recrystallized grain size. Geology **35**(4), 343–346 (2007). doi:10.1130/G23244A.1. http://geology.gsapubs.org/content/35/4/343.abstract

S. Balay, S. Abhyankar, M.F. Adams, J. Brown, P. Brune, K. Buschelman, V. Eijkhout, W.D. Gropp, D. Kaushik, M.G. Knepley, L.C. McInnes, K. Rupp, B.F. Smith, H. Zhang, PETSc Users Manual, Technical Report ANL-95/11 - Revision 3.5, Argonne National Laboratory, 2014. `http://www.mcs.anl.gov/petsc`

G.G. Bratu, Sur les quations intgrales non linaires. Bulletin de la Socit Mathmatique de France **42**, 113–142 (1914)

O. Coussy, *Poromechanics*, 2nd edn. (Wiley, Chichester, 2004)

A.C. Fowler, X.-S. Yang, Dissolution/precipitation mechanisms for diagenesis in sedimentary basins. Journal of Geophysical Research: Solid Earth **108**(B10), (2003). 2509. doi:10.1029/2002JB002269

D. Gaston, C. Newman, G. Hansen, D. Lebrun-Grandi, Moose: A parallel computational framework for coupled systems of nonlinear equations. Nuclear Engineering and Design **239**(10), 1768–1778 (2009). doi:10.1016/j.nucengdes.2009.05.021

I.J. Gruntfest, Thermal feedback in liquid flow; plane shear at constant stress. Journal of Rheology **7**(1), 195–207 (1963). doi:10.1122/1.548954

M.R. Handy, Flow laws for rocks containing two non-linear viscous phases: A phenomenological approach. Journal of Structural Geology **16**(3), 287–301 (1994). doi:http://dx.doi.org/10.1016/0191-8141(94)90035-3. http://www.sciencedirect.com/science/article/pii/0191814194900353

M. Herwegh, T. Poulet, A. Karrech, K. Regenauer-Lieb, From transient to steady state deformation and grain size: A thermodynamic approach using elasto-visco-plastic numerical modeling. Journal of Geophysical Research:

Solid Earth **119**(2), 900–918 (2014). 2013JB010701. doi:10.1002/2013JB010701. http://dx.doi.org/10.1002/2013JB010701

M. Herwegh, J.-P. Hürzeler, O.A. Pfiffner, S.M. Schmid, R. Abart, A. Ebert, The glarus thrust: excursion guide and report of a field trip of the swiss tectonic studies group (swiss geological society, 14.–16. 09. 2006). Swiss Journal of Geosciences **101**(2), 323–340 (2008). doi:10.1007/s00015-008-1259-z

H.D. Hibbitt, B.I. Karlsson, I. Sorensen, *ABAQUS/Standard – User's Manual Version 6.7* (Hibbit, Karlsson and Sorenson Inc., Pawtucket, 2008)

M. Huang, P.E.J. Rivera-Daz-del-Castillo, O. Bouaziz, S. van der Zwaag, Modelling the steady state deformation stress under various deformation conditions using a single irreversible thermodynamics based formulation. Acta Materialia **57**(12), 3431–3438 (2009). doi:http://dx.doi.org/10.1016/j.actamat.2009.03.023. http://www.sciencedirect.com/science/article/pii/S1359645409001748

B.S. Kirk, J.W. Peterson, R.H. Stogner, G.F. Carey, libMesh : a C++ library for parallel adaptive mesh refinement/coarsening simulations. Engineering with Computers **22**(3-4), 237–254 (2006). doi:10.1007/s00366-006-0049-3

D.A. Knoll, D.E. Keyes, Jacobian-free NewtonKrylov methods: a survey of approaches and applications. Journal of Computational Physics **193**(2), 357–397 (2004). doi:10.1016/j.jcp.2003.08.010

F. Oka, S. Kimoto, Y. Higo, H. Ohta, T. Sanagawa, T. Kodaka, An elasto-viscoplastic model for diatomaceous mudstone and numerical simulation of compaction bands. International Journal for Numerical and Analytical Methods in Geomechanics **35**(2), 244–263 (2011). doi:10.1002/nag.987

P. Perzyna, Fundamental problems in viscoplasticity. Adv. Appl. Mech. **9**, 243–377 (1966)

T. Poulet, K. Regenauer-Lieb, A. Karrech, L. Fisher, P. Schaubs, Thermal-hydraulic-mechanical-chemical coupling with damage mechanics using ES-CRIPTRT and ABAQUS. Tectonophysics **526-529**(0), 124–132 (2012). doi:10.1016/j.tecto.2011.12.005

T. Poulet, E. Veveakis, K. Regenauer-Lieb, D.A. Yuen, Thermo-poro-mechanics of chemically active creeping faults: 3. the role of serpentinite in episodic tremor and slip sequences, and transition to chaos. Journal of Geophysical Research: Solid Earth **119**(6), 4606–4625 (2014). doi:10.1002/2014JB011004

T. Poulet, M. Veveakis, A viscoplastic approach for pore collapse in saturated soft rocks using redback: An open-source parallel simulator for rock mechanics with dissipative feedbacks. Computers and Geotechnics **74**, 211–221 (2016). doi:http://dx.doi.org/10.1016/j.compgeo.2015.12.015. http://www.sciencedirect.com/science/article/pii/S0266352X15002785

T. Poulet, M. Paesold, E. Veveakis, Multi-physics modelling of fault mechanics using red-back - a parallel open-source simulator for tightly coupled problems. Rock Mechanics and Rock Engineering (2016 (in press)). doi:10.1007/s00603-016-0927-y

T. Poulet, M. Veveakis, M. Herwegh, T. Buckingham, K. Regenauer-Lieb, Modeling episodic fluid-release events in the ductile carbonates of the glarus thrust. Geophysical Research Letters **41**(20), 7121–7128 (2014). doi:10.1002/2014GL061715

M.M. Rashid, Incremental kinematics for finite element applications. International Journal for Numerical Methods in Engineering **36**(23), 3937–3956 (1993). doi:10.1002/nme.1620362302

K. Regenauer-Lieb, M. Veveakis, T. Poulet, F. Wellmann, A. Karrech, J. Liu, J. Hauser, C. Schrank, O. Gaede, M. Trefry, Multiscale coupling and multiphysics approaches in earth sciences: Applications. Journal of Coupled Systems and Multiscale Dynamics **1**(3), 281–323 (2013). doi:10.1166/jcsmd.2013.1021

J.R. Rice, N. Lapusta, K. Ranjith, Rate and state dependent friction and the stability of sliding between elastically deformable solids. Journal of the Mechanics and Physics of Solids **49**(9), 1865–1898 (2001). The {JW} Hutchinson and {JR} Rice 60th Anniversary Issue. doi:10.1016/S0022-5096(01)00042-4

K.H. Roscoe, J.B. Burland, On the generalised stress–strain behaviour of wet clay, in *Engineering Plasticity*, ed. by J. Heyman, F.A. Leckie (Cambridge University Press, ???, 1968), pp. 535–609

p. Succombe, Succombe, a spectral coupled multiphysics and mechanics bifurcation method: pseudo arclength continuation and computational singular perturbation method. ??? (2015)

J. Sulem, V. Famin, Thermal decomposition of carbonates in fault zones: slip-weakening and temperature-limiting effects. J. Geophys. Res. **114**, 03309 (2009). doi:10.1029/2008JB006004.

J. Taron, D. Elsworth, K.-B. Min, Numerical simulation of thermal-hydrologic-mechanical-chemical processes in deformable, fractured porous media. International Journal of Rock Mechanics and Mining Sciences **46**(5), 842–854 (2009). doi:10.1016/j.ijrmms.2009.01.008

G. Taylor, H. Quinney, The latent energy remaining in a metal after cold working. Proc. R. Soc., Ser. A. **143**, 307–326 (1934)

I. Vardoulakis, J. Sulem (eds.), *Bifurcation Analysis in Geomechanics* (Blankie Acc. and Professional, ???, 1995)

P. Varotsos, K. Alexopoulos, Negative activation volumes of defects in solids. Phys. Rev. B **21**, 4898–4899 (1980). doi:10.1103/PhysRevB.21.4898

E. Veveakis, S. Alevizos, I. Vardoulakis., Chemical reaction capping of thermal instabilities during shear of frictional faults. J. Mech. Phys. Solids **58**, 1175–1194 (2010). doi:10.1016/j.jmps.2010.06.010.

E. Veveakis, T. Poulet, S. Alevizos, Thermo-poro-mechanics of chemically active creeping faults: 2. transient considerations. Journal of Geophysical Research: Solid Earth **119**(6), 4583–4605 (2014). doi:10.1002/2013JB010071

E. Veveakis, T. Poulet, M. Paesold, S. Alevizos, K. Regenauer-Lieb, The role of diagenetic reactions during fluid flow through nominally impermeable shales. Rock Mechanics and Rock Engineering **Submitted** (2015)

R. Weinberg, M. Veveakis, K. Regenauer-Lieb, Compaction-driven melt segregation in migmatites. Geology **43**(6) (2015). (in press). doi:10.1130/G36562.1

C. Zhu, P. Lu, Alkali feldspar dissolution and secondary mineral precipitation in batch systems: 3. saturation states of product minerals and reaction paths. Geochimica et Cosmochimica Acta **73**(11), 3171–3200 (2009). doi:10.1016/j.gca.2009.03.015